Clemens Bender, BSc

Long-Term Stable Phosphoric Acid Tolerant Electrocatalysts for High Temperature PEM Fuel Cell Applications

MASTER'S THESIS

to achieve the university degree of

Diplom-Ingenieur

Master's degree programme: Technical Chemistry

submitted to

Graz University of Technology

Supervisor

Assoc.Prof. Dipl.-Ing. Dr.techn., Viktor Hacker

Institute of Chemical Engineering and Environmental Technology

Dipl.-Ing BSc Katharina Kocher

Graz, November 2017

AFFIDAVIT

I declare that I have authored this thesis independently, that I have not used other than the declared sources/resources, and that I have explicitly indicated all material which has been quoted either literally or by content from the sources used. The text document uploaded to TUGRAZonline is identical to the present master‘s thesis.

Date

Signature

Acknowledgements

First and foremost I would like to thank Assoc. Prof. Viktor Hacker for the opportunity to write this master's thesis under his supervision and for his support and advice during the preparation of this work.

Special thanks go to DI Dr. Alexander Schenk. I am very grateful to Alexander for his expert guidance during the preparation of this thesis and for his creative input and support. Your encouragement and dedication during this time was always greatly appreciated.

Special thanks go to DI Katharina Kocher for her advice and for her patience during the evaluation of this work.

Furthermore, I would like to thank the entire fuel cell working group for the friendly and supportive environment. I am thankful for your constant assistance and for sharing your experience with me.

Finally I would like to thank my family for moral and financial support during the entirety of my studies. Without you this work would not have been possible.

Abstract

A prerequisite for the successful commercialisation of high-temperature polymer electrolyte membrane fuel cells (HT-PEMFCs) is the cost reduction of the system. In order to catalyse the kinetically slow oxygen reduction reaction (ORR) and to ensure high performance and a long lifetime of the catalyst, high loadings of the expensive precious metal platinum (Pt) are needed. The phosphate species, that are present in the fuel cell's membrane, limit the performance of the catalyst by adsorption on its active sites. An effective method to stabilise the catalyst and protect its surface against phosphate poisoning is needed to facilitate the reduction of the amount of Pt and thus the price of the system.

Conductive polymers such as polyaniline (PANI) have been shown to not only have a positive effect on the activity of the catalyst but also effectively protect the catalyst from poisoning.

In this work Pt based catalysts were functionalised with PANI using a straightforward and inexpensive preparation method. High surface carbon was impregnated with a precursor solution containing Pt salt. After reduction of the salt to Pt nanoparticles (NPs), a thin layer of PANI was deposited on the catalyst particles by oxidative polymerisation of aniline. Using a similar method, high surface carbon was functionalised with PANI and platinum NPs were then deposited on the PANI decorated carbon support. The catalysts were characterised using a rotating disk electrode. Additionally, pre-prepared gas diffusion electrodes were functionalised with PANI and investigated in single cells.

Ex-situ and in-situ experiments showed an increase in activity and stability of the catalysts after functionalisation with PANI. The in-situ measurements revealed that PANI significantly improved the long term stability and overall activity of the catalysts.

Kurzfassung

Eine Voraussetzung für die erfolgreiche Kommerzialisierung von Hochtemperatur Polymerelektrolyt Brennstoffzellen (HT-PEMFC) ist die Senkung der Anschaffungskosten des Systems. Hohe Platinbeladungen sind nötig, um die kinetisch gehemmte Sauerstoffreduktionreaktion (ORR) zu katalysieren und eine langzeitstabile Brennstoffzelle zu gewährleisten. Phosphatspezies, die in der Polymerelektrolytmembran vorkommen, können die aktive Oberfläche des Katalysators blockieren und seine Aktivität verringern. Um die Platinbeladung und einhergehend die Kosten des Systems zu reduzieren, ist ein Schutz der Katalysatoroberfläche mit Hilfe einer wirkungsvollen Methode notwendig.

Leitfähigen Polymeren wie Polyanilin (PANI) wurde nachgewiesen, dass sie die Aktivität des Katalysators erhöhen und zusätzlich die Nanopartikel vor Katalysatorgiften schützen.

In dieser Arbeit wurden Platinkatalysatoren mittels einer kostengünstigen Methode mit PANI funktionalisiert. Kohlenstoff wurde mit einer Platinsalzlösung imprägniert. Nach der Reduktion zu Pt Nanopartikeln (NP) wurde durch oxidative Polymerisation eine dünne Schicht PANI auf der Oberfläche der Katalysatorpartikel abgeschieden. Mit einer ähnlichen Methode wurde Kohlenstoff mit PANI funktionalisiert. Pt-NP wurden anschließend auf diesem funktionalisierten Kohlenstoff abgeschieden und anschließend mittels rotierender Scheibenelektrode (RDE) charakterisiert. Zusätzlich wurden vorgefertigte Gasdiffusionselektroden (GDE) mit PANI funktionalisiert und in Einzelzellmessungen charakterisiert.

Die ex-situ und in-situ Ergebnisse zeigen, dass die Katalysatoren nach der PANI-Behandlung eine erhöhte Stabilität und Aktivität aufweisen. Die Einzelzellmessungen zeigen überdies eine deutlich verbesserte Langzeitstabilität und Aktivität der funktionalisierten Elektroden.

Abbreviations

AL	Active layer
APS	Ammonium persulfate
CE	Counter electrode
CV	Cyclic voltammetry
ECSA	Electrochemical active surface area
EtOH	Ethanol
Eq.	Equation
FC	Fuel cell
GDE	Gas diffusion electrode
GDL	Gas diffusion layer
HHV	Higher heating value
HT	High temperature
HOR	Hydrogen oxidation reaction
IPA	Isopropyl alcohol
LHV	Lower heating value
LT	Low temperature
MA	Mass activity
MEA	Membrane electrode assembly
OCV	Open circuit voltage

ORR	Oxygen reduction reaction
P_{Ref}	Power density using reformate H_2
PA	Phosphoric acid
PANI	Polyaniline
PBI	Polybenzimidazole
PEM	Polymer electrolyte membrane
PEMFC	Polymer electrolyte membrane fuel cell
PFSA	Perflourosulfanic acid polymer
Pt	Platinum
NP	Nanoparticle
Pt/C	Carbon supported platinum catalyst
Pt/C@PANI20	Carbon supported PANI decorated platinum catalyst
$Pt_{30}Co/C$	Carbon supported platinum cobalt catalyst
$Pt_{30}Co/C@PANI20$	Carbon supported PANI decorated platinum cobalt catalyst
RDE	Rotating disk electrode
RHE	Reversible hydrogen electrode
SCD	Specific current density
WE	Working electrode

Content

1 Introduction

Limiting the effects of global warming and meeting the 2 °C goal set by the Paris climate agreement[1] is one of the biggest ecological and socio-ecological challenges of our time. The correlation between the earth's surface temperature and the CO_2 concentration in the atmosphere is undeniable proof of the human influence on climate change caused by green-house-gas emissions. Considering the facts of depleting supplies of carbon based fossil fuels and the projected increase in the world's energy demand of 48% between the years 2012 and 2040[2], the challenge of green-house-gas reduction while satisfying energy needs must be met with increased use of low-carbon and carbon-free energy sources such as renewables.

However, the majority of renewable sources of electricity (e.g. solar, wind, hydropower etc.) suffer from fluctuation which in turn can destabilises the power grids. This circumstance limits the integration of renewable energy into the electricity system to approx. 20-25%.[3] Further implementation of renewable energy into the electricity system is only possible by sophisticated energy storage and conversion technologies.

Fuel cells (FCs) offer a promising and environmentally friendly pathway for the generation of clean electricity on demand. They convert the stored energy of the fuel electrochemically by combining oxygen (O_2) and hydrogen (H_2) to form water (H_2O) and emission free electricity with high efficiency. Especially with fuels produced from renewable resources, nearly carbon-neutral energy generation can be achieved. FCs have a wide range of applications, from stationary power plants to smaller units for the automotive sector and portable devices.[4] In particular, high temperature polymer electrolyte FCs (HT-PEMFCs) have gained much attention due to their relatively high tolerance towards impurities in the fuel which simplifies the H_2 purification process. Downsides of HT-PEMFCs include the necessity of high platinum (Pt) loadings due to the sluggish kinetics of the oxygen reduction reaction (ORR). A second drawback of HT-PEMFCs is the presence of phosphoric acid (H_3PO_4, PA) in the FC. Several phosphate species can adsorb on the Pt catalyst and decrease its catalytic activity. The adsorption of phosphates on the Pt surface, known as catalyst poisoning, limits the lifetime of HT-PEMFCs significantly.

In consideration of the problems concerning the stability of Pt catalysts used in HT-PEMFCs, this work was aimed at mitigating the issue of catalyst poisoning caused by phosphates. In an

attempt to improve the stability and catalytic activity of Pt, Pt based catalysts were functionalised with polyaniline (PANI). PANI is an organic polymer effectively protects the catalyst's active sites against phosphate poisoning. The PANI is prepared by selectively adsorbing aniline monomer units on the surface of the catalyst nanoparticles (NPs), specifically on the carbon support material. After an oxidative polymerisation of the monomers the NPs are covered with a thin film of PANI, creating a core-shell type structure.[5]

In this work, commercial and in-house Pt based catalysts were functionalised with PANI. Their catalytic activity and stability was compared with their non-functionalised counterparts in ex-situ measurements. Additionally, pre-prepared gas diffusion electrodes (GDEs) were decorated with PANI and tested in-situ in single cells. Their catalytic activity and their long term stability are investigated and compared to that of electrodes without PANI.

2 Theory

2.1 Fuel Cell Fundamentals

The underlying principle for FCs stands out due to its simplicity. In contrast to internal combustion engines (ICEs), where the fuel's chemical energy is converted into mechanical energy by use of combustion, FCs convert energy electrochemically. H_2 and an oxidant (e.g. O_2 or air) are catalytically converted into electricity and heat by means of an electrochemical reaction occurring at the respective electrodes, the anode and the cathode.[6] At the anode, H_2 is oxidised while at the cathode, O_2 is reduced. The overall reaction as well as the reactions at the anode and the cathode are listed in Table 1.

Table 1: Overall reaction and reactions at the two electrodes of a FC.

Overall reaction	$H_2 + \frac{1}{2}O_2 \rightarrow H_2O$	Eq. 2-1
Anode reaction	$H_2 \rightarrow 2H^+ + 2e^-$	Eq. 2-2
Cathode reaction	$O_2 + 2e^- \rightarrow 2O^-$	Eq. 2-3

Table 2.1 shows the most important types of FCs, their common operating temperatures and their respective mobile ions. While the entire listed types share the overall reaction Eq. 2-1, some FCs exhibit elaborate reaction pathways. In particular, direct FCs which utilize methanol or ethanol as liquid fuel, exhibit a number of complex reaction steps and intermediate products.[7] These cells, while being a candidate for mobile and portable applications, suffer from low power caused in part by methanol diffusion through the membrane from the anode to the cathode, resulting in significantly diminished cell potentials.[6]

The most promising candidate for mobile applications is the polymer electrolyte membrane FC (PEMFC). PEMFCs feature a solid electrolyte membrane, allowing for tight fuel cell stack builds and highly compact systems. High power densities as well as short start-up times are also key advantages of PEMFCs over other types of FCs.

Table 2: Fuel cell types with operating temperature and mobile ions.[6]

Fuel cell type	*Operating temperature*	*Mobile ion*
Polymer Electrolyte Membrane Fuel Cell (PEMFC)	60 - 180 °C	H^+
Alkaline Fuel Cell (AFC)	50 – 200 °C	OH^-
Direct Methanol Fuel Cell (DMFC)	20 - 90 °C	H^+
Phosphoric Acid Fuel Cell (PAFC)	~220 °C	H^+
Molten Carbonate Fuel Cell (MCFC)	~650 °C	CO_3^{2-}
Solid Oxide Fuel Cell (SOFC)	500 – 1000 °C	O^{2-}

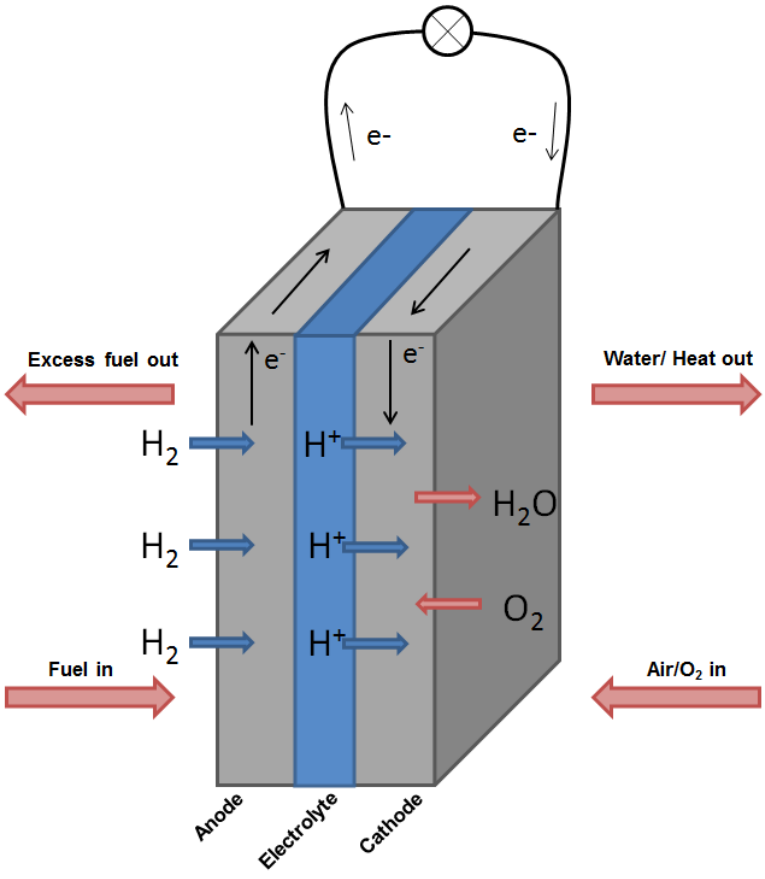

Figure 1: Schematic of a PEMFC.[8]

Figure 1 shows the scheme of a PEMFC. The solid polymer electrolyte membrane (PEM) is sandwiched between the two electrodes, a build-up which is called the membrane electrode assembly (MEA). The electrodes themselves are made up of a gas diffusion layer (GDL) and an

active layer (AL). The GDL's allows for the unhindered diffusion and even distribution of the gases, H_2 and air/O_2 to the anode and the cathode respectively. Its second task is the transport of electrons generated during the reaction. For these purposes and due to the need of mechanical stability, the GDL is most often made of carbon cloth or carbon paper. The AL is made up of the catalyst as well as the support material, usually high surface carbon, and is in direct contact with the membrane in the MEA. The membrane is made from ion conducting polymers and, as well as being electrically insulating, acts as a separator for the gases.

The three-phase-boundary is the contact area of the three materials in the MEA, the GDL, the AL and the membrane. It is the intersection of fuel/oxidant, catalyst and membrane and is the area where the electrochemical reaction takes place. Maximising this intersection of all three phases is crucial for the performance of a FC.

For a FC, the maximum electrical work ΔG^0 obtainable at constant temperature and pressure can expressed as in Eq. 2-4.[9]

$$\Delta G^0 = -nFE_{th} \qquad \text{Eq. 2-4}$$

ΔG^0	Molar Gibbs free energy of liquid water	(273.34 kJ mol^{-1})
n	Number of electrons	
F	Faradays constant	(96485 C mol^{-1})
E_{th}	Theoretical cell voltage	

Assuming that the FC produces liquid water and operates at 25 °C with pure O_2 and H_2 at 1 atm, the theoretical cell voltage E_{th} can be expressed as in Eq. 2-5.[6]

$$E_{th} = \frac{\Delta G^0}{-nF} = 1.23V \qquad \text{Eq. 2-5}$$

However, certain voltage losses occur under real operatin conditions, causing the actual cell voltage E_{cell} to diminish as shown in Eq. 2-6. Figure 2 depicts a typical polarisation curve of a FC and illustrates the losses which occur during operation.

$$E_{cell} = E_{rev} - \Delta E_{Ohm} - \eta_{ORR} - \eta_{MT} \qquad \text{Eq. 2-6}$$

E_{rev}	Reversible cell voltage
ΔE_{Ohm}	Voltage losses due to ohmic resistances
η_{ORR}	Overpotential due to slow ORR kinetics
η_{MT}	Overpotential due to mass transport limitations

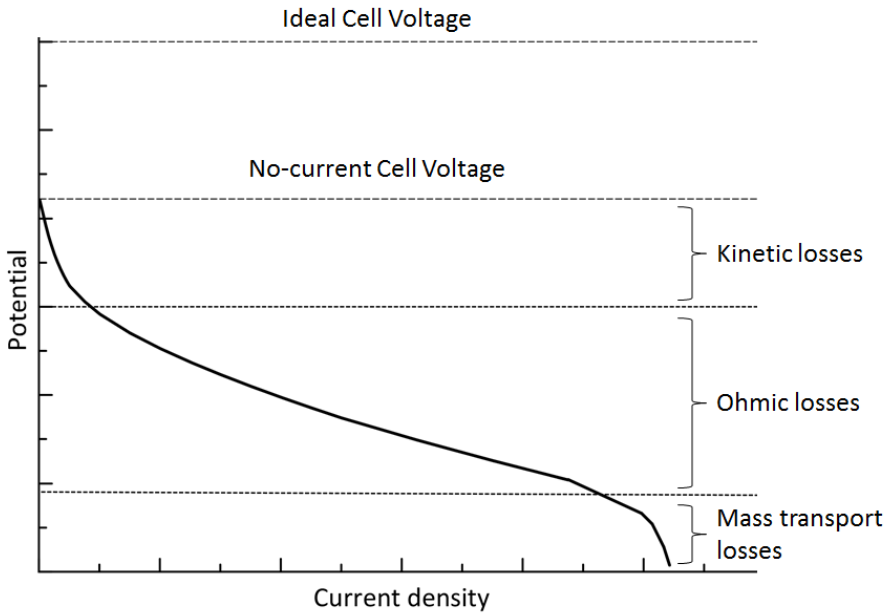

Figure 2: Potential losses of a PEMFC during operation.[10]

The efficiency of FCs may be expressed as the ratio of Gibbs free energy ΔG and the enthalply ΔH. Two enthalpies must be considered, depending on the operating conditions and the state of the product water. In the case of gaseous water ΔH_{LHV} is used whereas for liquid water ΔH_{HHV} is used.

With these values, the ideal efficiency η_{ideal} of a FC can be expressed (Eq. 2-8 and Eq. 2-8).

$$\eta_{ideal}^{LHV} = \frac{\Delta G}{\Delta H_{LHV}} = 94.5\% \qquad \text{Eq. 2-7}$$

$$\eta_{ideal}^{HHV} = \frac{\Delta G}{\Delta H_{HHV}} = 83.1\% \qquad \text{Eq. 2-8}$$

ΔH_{LHV} Enthalpy based on the lower heating value when gaseous water is produced (241.2 kJ mol^{-1})

ΔH_{HHV} Enthalpy based on the higher heating value when liquid water is produced (285.6 kJ mol^{-1})

Under normal operating conditions the efficiency may also be expressed as in Eq. 2-9.

$$\eta_{ideal} = \frac{\mathrm{E}_{real}}{\mathrm{E}_{th}} \qquad \text{Eq. 2-9}$$

2.2 High Temperature PEMFCs

In contrast to LT-PEMFCs which are operated at around 80 °C, HT-PEMFCs are operated at temperatures of 100-200 °C. The operation at higher temperatures brings several advantages of HT-PEMFCs over LT-PEMFCs.

One important benefit of HT-PEMFCs is the simplified water managements compared LT-PEMFCs. In LT-PEMFCs NAFION®, which consists of fluorosulfonated ionomers (perfluorosulfonic acid, PFSA), is usually used as membrane. This type of membrane needs accurately adjusted humidity, usually by humidification of the reaction gases, for optimal performance and long lifetime.[11] Thus, high water content and a complicated humidification system is needed in those FCs. In HT-PEMFCs, PA doped polybenzimidazole (PBI) is used as membrane material which makes the operation at temperatures of up to 200 °C possible without additional humidification of the reaction gases.[10] The PBI possesses high conductivity and is stable at temperatures of up to 200 °C.[12] The structure of PBI is shown in Figure 3.

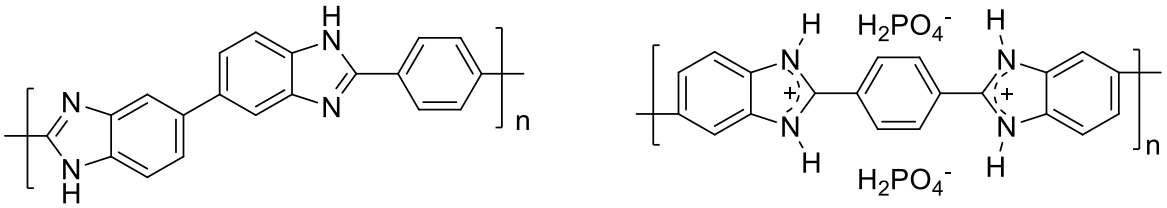

Figure 3: Structure of PBI (left) and PA doped PBI (right).

Due to the higher temperatures the heat management in HT-PEMFCs is simplified. Since the underlying reaction of H_2 and O_2 to H_2O is exothermic, the generated heat needs to be dissipated in the case of LT-PEMFCs as the system temperature would rise above the regular operating temperature. In high temperature operation, cooling may be minimal and the excess heat may be used for the generation of warm water or steam. In addition to lower system cost due to the lack of a cooling system, using the generated heat for applications such as the generation of warm water also increases the overall system efficiency.[13,14]

The elevated operating temperatures also reduce problems concerning catalyst poisoning. The interactions of catalysts poisons such as CO with the Pt-based catalyst are considerably weaker at higher temperatures and so the margin for impurities in the fuels is larger, resulting in easier and inexpensive fuel purification.[15–17]

The significant advantage of HT-PEMFCs over LT-PEMFCs is posed by the enhanced reaction kinetics. The hydrogen oxidation reaction (HOR) at the anode generally occurs much quicker than the ORR at the cathode. This way, the ORR determines the overall reaction kinetics. At elevated temperatures it becomes easier for the reactants to overcome the activation energy (E_A) of the reaction and thus the reaction rate is higher.[18]

The high temperatures along with the relatively low degree of humidity create a harsh environment for the components of the FC. Pt, though being highly stable and active towards the ORR, suffers from several phenomena affecting its catalytic performance. The dissolution of Pt under harsh conditions limits the lifetime of FCs significantly as the catalyst is irreversibly lost from the AL in the cell.[19] Under these conditions, the degradation and agglomeration of the catalyst takes place at a higher rate than in LT-PEM FCs.[17] The use of a PA doped PBI membranes results in one important drawback as the PA tends to leach from the membrane into the cell in the form of several phosphate species, namely $H_2PO_4^-$, HPO_4^{2-} and PO_4^{3-}.[20] These species strongly adsorb on the catalyst, block the active sites and effectively diminish the surface area of the catalyst. Phosphate ions may compete with H_2, O_2 and hydroxide molecules (OH^-) for the adsorption sites of Pt and thus have negative impact on the performance of the ORR.[21] The overall coverage depends of the concentration of the phosphates as well as the orientation of the Pt crystals.[20]

Besides the aforementioned dissolution and poisoning of the catalyst, loss of the carbon support due to corrosion negatively affects the performance of the electrodes.

The mechanisms of catalysts agglomeration and phosphate poisoning are described as being the main source of performance losses in HT-PEM FCs.[17] Possible answers to these challenges include the alloying of Pt with non-precious metals and embedding the catalyst in a protective polymer layer. These solutions are presented in the following chapters 2.3 and 2.4.

2.3 Pt and Pt-alloy Catalysts

Although much effort has been put into the reduction of Pt loadings in FCs, further reductions are prerequisites for the successful commercialisation of FCs as Pt still accounts for approximately 30 % of FC manufacturing costs.[22] Especially on the cathode side of the FC, Pt is of great importance as it exhibits very high activity towards the ORR. Among the contributors to overpotential losses such as diffusion overpotentials and internal current overpotentials, the ORR is arguably the most decisive, accounting for approximately 0.3 V in voltage loss.[23] Novel Pt-alloy catalysts are a possible pathway for continued cost-cutting for the FC system not only due to their durability and activity but also due to their relative affordability.[24]

Pt-nickel (Pt-Ni) and Pt-cobalt (Pt-Co) alloy catalysts are among the most intensively investigated Pt-alloy catalysts. They have received much attention due to their effects of Pt-Pt bond distance, d-band shifts as well as surface and lattice effects attained by thermal or acid treatments.[25–27] These effects have been shown to play an important role in the adsorption of O_2 on the surface of the catalysts. The quality and degree of adsorption of O_2 is decisive for electron transfer kinetics and bond breaking rates.[26] The available surface area of the catalyst is also of great importance. In order to obtain Pt-alloy catalysts or, more specifically, Pt-Cobalt catalysts with very high surface areas, the catalysts are subjected to acid and heat treatment. Pt-Ni and Pt-Co alloys reportedly have higher tolerance towards CO poisoning than pure Pt catalysts. Pt-Ni has additionally been shown to be more tolerant towards phosphate poisoning than pure Pt.[21]

Figure 4 illustrates the acid-leaching process of a Pt-Co alloy catalyst. Cobalt atoms are dissolved by the acid to form a catalyst that exhibits a Pt-enriched surface with a very large area. However, cobalt atoms which are not dissolved in the bulk of the catalyst still maintain the lattice strain effects which positively influence the activity towards the ORR.[24]

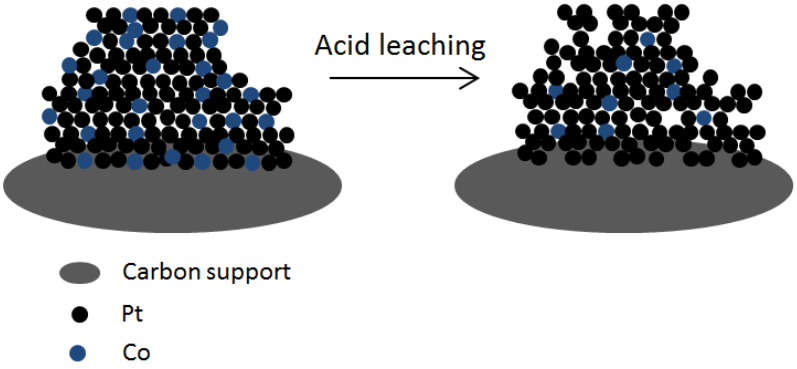

Figure 4: Schematic of an acid leaching process of a Pt-Co-alloy catalyst.[24]

2.4 Phosphoric Acid Tolerance and Catalyst Functionalisation

In an attempt to improve the durability and corrosion resistance of commercial carbon support, carbon nanostructures such as nanotubes, multi-walled-nanotubes and graphene have been investigated as support materials. Nitrogen doped carbon supports have additionally been shown to exhibit catalytic activity, albeit less so than their Pt and Pt-alloy counterparts.[28–30] In recent studies, nitrogen-bearing polymers such as polyaniline (PANI) have been investigated for FC applications. The intrinsic electron conductivity of such polymers in acidic environments offers promising improvements on conventional carbon support materials when the two materials are paired as in nitrogen-doped carbon supports.[28,31] In addition, electrodes manufactured with these nitrogen-doped carbon supports have reportedly improved their durability in FCs.[32]

Figure 5 shows the molecular structure of PANI. PANI is synthesised by oxidative coupling of aniline monomers. The polymer is built up of two different kinds of repeating units featuring different oxidation states. Next to its favourable electronic properties, PANI has unique redox properties and high environmental stability.[5]

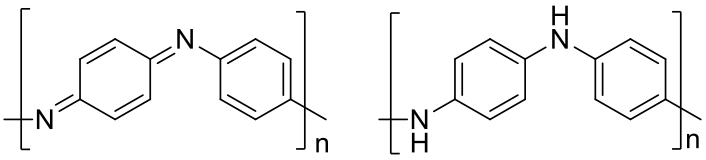

Figure 5: Molecular structure of PANI.

Chen et al. present an approach of catalyst functionalisation that tackles the challenges of both carbon corrosion and blocking of the catalyst's active sites by PA poisoning.[5] In the synthesis showcased in their work, aniline selectively adsorbs on the surface of the carbon support, on which Pt nanoparticles (NP) have been deposited, via π-π-conjugation.[5] After oxidative coupling of the aniline monomers via ammonium persulfate (APS) a PANI film is formed, ensheathing the carbon support. The PANI acts as a protecting film for the support material and thus prevents carbon corrosion by shielding the carbon from the corrosive environment of the FC.[5] A schematic of the synthesis of PANI on a carbon supported Pt catalyst (Pt/C) is shown in Figure 6.

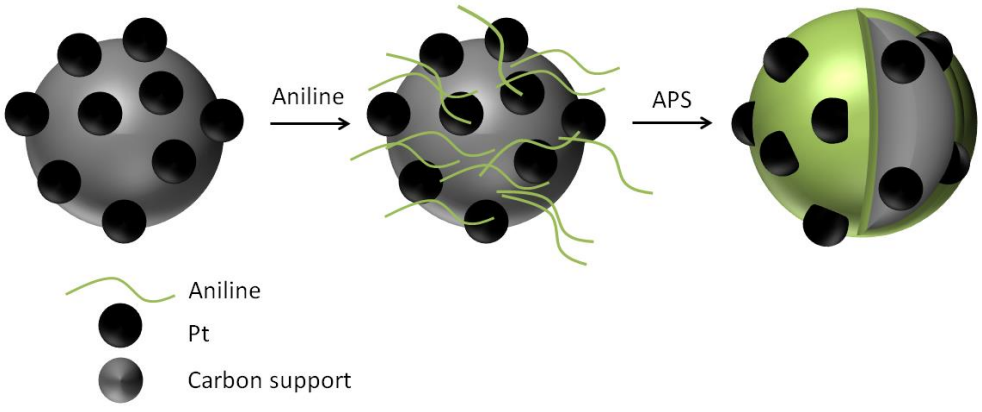

Figure 6: Schematic of the polyaniline-functionalisation of Pt/C.[5]

Due to the selective binding of the aniline on the carbon surface, most of the Pt-surface remains free of aniline, thus upholding its active surface. These catalysts show high activity towards the ORR that is strongly dependant on the thickness of the PANI layer formed.[5] The

thickness of the layer is proportional to the amount of aniline monomer used und can thus be quite accurately controlled. An overly thick layer of PANI can cause the Pt-particles to be covered alongside the support. This in turn diminishes the area of the catalyst and corrupts its performance.

Chen and co-workers report that the Pt/C catalysts functionalised with PANI (Pt/C@PANI) exhibited higher activity towards the ORR than their respective non-functionalised catalysts. In addition to their high activity, the PANI coated catalysts were reportedly also more electrochemically stable than the catalysts without PANI. Figure 7 illustrates the electrochemical active surface area (ECSA) of two catalysts, whereof on is functionalised with 30wt% PANI. After 1500 CV cycles the functionalised catalyst still exhibits 70% of its initial ECSA whereas the non-functionalised counterpart only has 20% of its initial ECSA.[5]

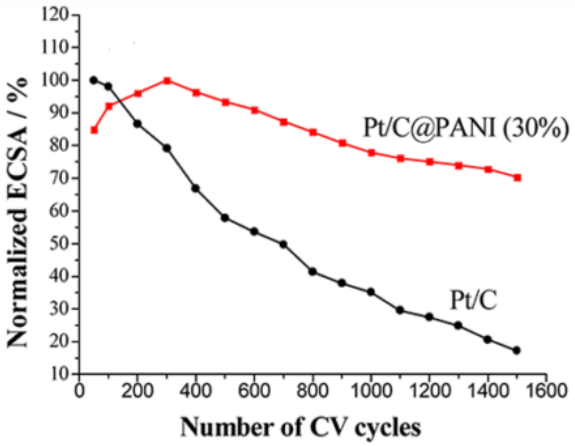

Figure 7: Normalized ECSAs of electrodes made with Pt/C and Pt/C@PANI (30wt%) catalysts as functions of the number of CV cycles in N_2-purged 0.5 M H_2SO_4 at room temperature.[5]

Chen and co-workers also report that after accelerated stress tests (ASTs) were performed on both the PANI-coated catalyst and non-coated catalyst, the PANI-bearing catalyst showed much higher activity towards the ORR and upheld 76% of its current density.[5]

This improvement in activity and durability is ascribed to several factors. First, the core-shell structure of the catalysts particles (Figure 6) is reported to enable a delocalisation between the d-orbitals of the Pt and the π-conjugated PANI, changing the electronic nature of the Pt NPs.[5] Secondly, since the carbon support is fully encased by the PANI, the polymer protects the carbon support from the electrolyte and thus prevents carbon oxidation. Lastly, the Pt

particles are immobilized in the core shell structure by the PANI which impedes the agglomeration of Pt. [5]

In this work, functionalisation of Pt/C with PANI was performed analogously to the method described by Chen et al. In an attempt to improve upon said method, a second synthetic route was followed to fabricate PANI functionalised Pt/C. For this purpose, Vulcan was first decorated with PANI. Pt NPs were then deposited on the functionalised support material. This method was thought to make the synthesis more suitable and improve upon the existing method since it would ensure the entirety of the carbon support to be encapsulated by the PANI. Additionally, the performance of PANI decorated Pt based catalysts is reportedly strongly dependant on the thickness of the PANI layer since an overly thick film may cover the Pt NPs surface, hindering its catalytic effect. With a carbon support already decorated with PANI, the Pt NPs deposited will not be ensheathed and thus can exert their full catalytic performance.

2.5 Catalyst Characterisation via RDE

The rotating disk electrode (RDE) is an important tool for ex-situ characterisation of catalysts. In this method, an electrochemical cell is subjected to potentio-dynamic cycling and the resulting current is recorded. The setup for this method is shown in Figure 8. RDE experiments are carried out using a standard three-electrode setup comprised of a reference electrode (RE), a counter electrode (CE) and a working electrode (WE). The WE consists of a glassy carbon electrode recessed in a polytetrafluoroethylene (PTFE) sheath which is installed on a motor-driven rotating shaft. For this method, a suspension of the catalyst to be investigated is formed, usually with a mixture of isopropyl alcohol (IPA) and H_2O as the liquid phase.

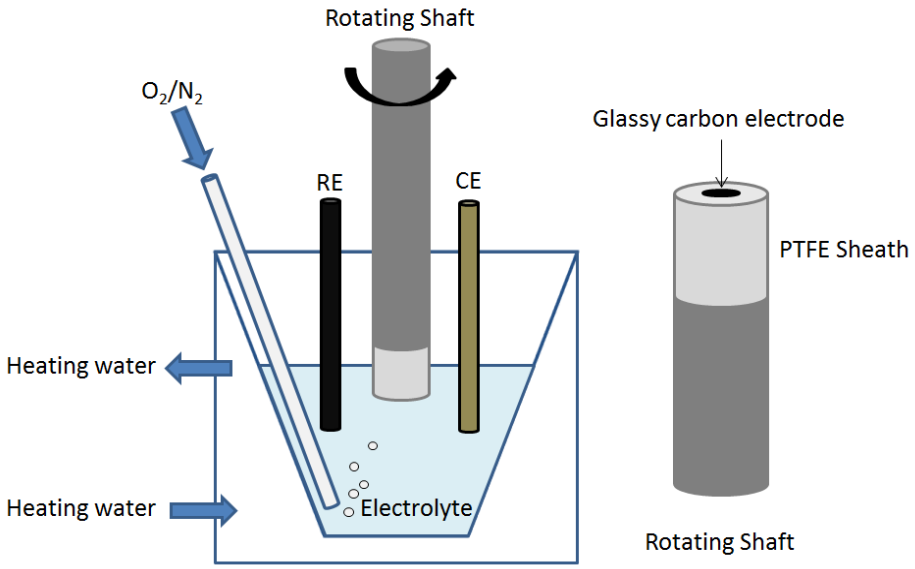

Figure 8: Standard RDE setup with three-electrode assembly.

The ink is dropped on the glassy carbon electrode. Upon rotation of the electrode, the ink dries, leaving behind a thin film of a known amount of catalyst on the electrode. Perchloric acid ($HClO_4$) is usually used as electrolyte as it shows minimal poisoning of the catalyst.[21] For catalyst characterisation, the electrolyte is purged with gases such as N_2 or O_2 and the disk electrode is inserted into the electrolyte. In order to obtain reproducible data from RDE measurements, each catalyst undergoes potential cycling until a stable potential is attained. In inert electrolyte, cyclic voltammetry (CV) experiments are performed to evaluate the active area of each catalyst. Figure 9 shows a typical cyclovoltammogramm (CV) of Pt-based catalyst. The shaded area Q_H of the curve corresponds to the charge needed for the adsorption of H_2 to the Pt surface. With the use of the literature value of charge needed to adsorb H_2 on 1 cm^2 of polycrystalline Pt (210 µC), the ECSA of the catalyst can be calculated according to Eq. 2-10.[33]

When recording the CV with and without contaminants in the electrolyte, the resulting ECSAs may be compared. From these comparisons, conclusions about the degree of contamination of the catalyst can be drawn. When PA is added to the electrolyte, the ECSA of the CV will usually decrease due to blocking of the active sites of the Pt catalyst by PA.

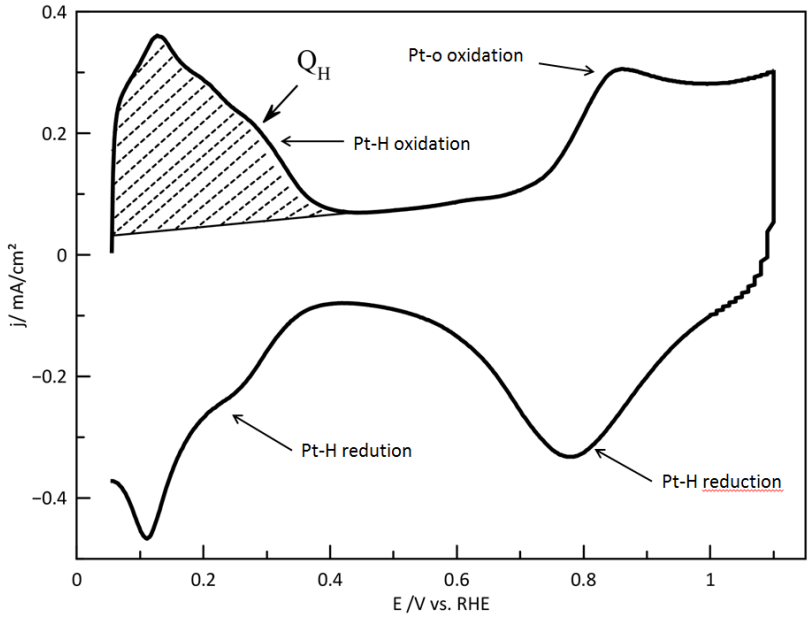

Figure 9: Cyclic voltammogram for Pt/C in acidic electrolyte.[33]

$$A_{active} = \frac{Q_H}{210\mu C} \qquad \text{Eq. 2-10}$$

$$ECSA = \frac{A_{active}}{l_{Pt}\, A_{RDE}} \qquad \text{Eq. 2-11}$$

l_{Pt}	Pt loading on the electrode	[mg]
A_{RDE}	Geometric area of the RDE	[cm²]

In O_2 purged electrolyte, the ORR polarisation curve is recorded. The obtained data are corrected with the previously recorded CV to obtain the corrected ORR polarisation curve. The CV, the as-obtained ORR and the corrected ORR are shown in Figure 10.

From the ORR, important parameters such as the specific current density (SCD), the mass activity (MA) and the number of electrons exchanged during each half-reaction, can be obtained. The latter is an important characteristic for the performance of the catalyst, the reaction pathway and its mechanism.[34]

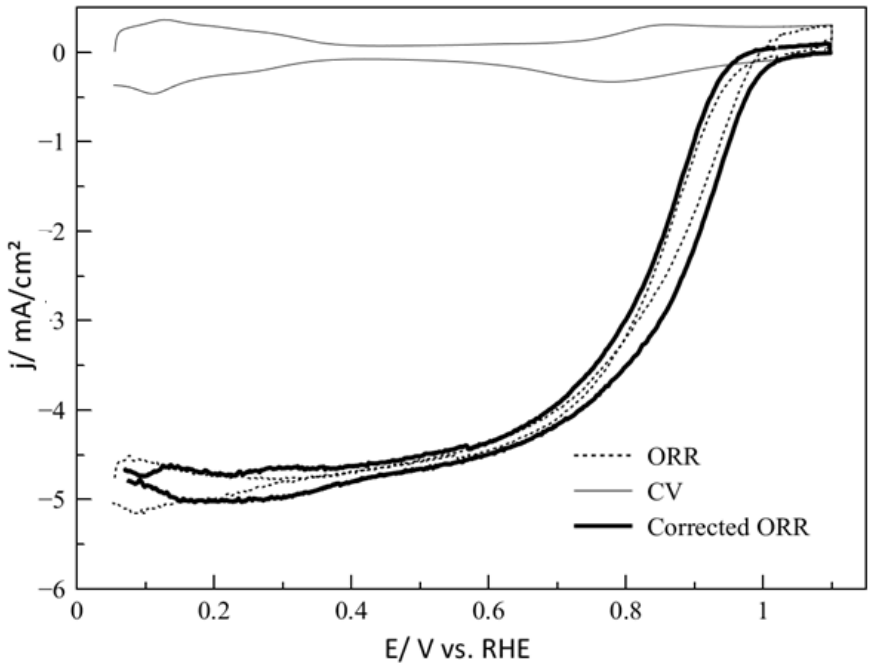

Figure 10: CV, as-recorded ORR and corrected ORR of Pt/C.

Eq. 2-12 and Eq. 2-13 represent the determination of the SCD and the MA.

$$SCD = \frac{i_d \cdot i}{i_d - i} \cdot \frac{1}{ECSA} \qquad \text{Eq. 2-12}$$

$$MA = i_k \frac{1}{l_{Pt}} \qquad \text{Eq. 2-13}$$

i_k	Kinetic limited current	[mA]
i_d	Diffusion limited current	[mA]
i	Current at 0.9 V	[mA]

For the calculation of the electron transfer number, the Levich analysis is carried out. For this purpose, the ORR is recorded at varying rotation speeds. Based on the Levich-equation the

diffusion limited current is plotted against the square root of the rotation speed (Eq. 2-14). From the slope of the resulting straight, the number of electrons n can be calculated.

$$i_l = -0.62 \cdot n \cdot F \cdot A \cdot D_R^{2/3} \cdot \omega^{1/2} \cdot v^{-1/6} \cdot C_R \qquad \text{Eq. 2-14}$$

n	Number of electrons	
F	Faradays constant	[96485 C mol^{-1}]
A	Area of electrode	[0.196 cm^2]
D_R	Diffusion coefficient	[1.9·10^{-5} cm^2 s^{-1}]
ω	Rotation of electrode	[rad s^{-1}]
v	Kinematic viscosity	[8.93·10^{-3} cm^2 s^{-1}]
C_R	Bulk concentration of O_2	[1.18·10^{-6} mol cm^{-3}]
i_l	Diffusion limited current	[A]

Although many valuable parameters of catalysts can be investigated using RDE experiments, the results from this method are not always applicable to the performance of the catalysts in FCs or FC stacks. Thus, for further investigation, in-situ experiments in single cells or stacks must be carried out.

3 Experimental

3.1 Materials and Methods

3.1.1 Chemicals

All chemicals were used as purchased without further purification.

- $H_2PtCl_6 \cdot 6H_2O$, metal basis 99.95%, Pt 39.72%, Alfa Aesar Premion®
- $Co(NO_3)_2 \cdot 6H_2O$, metal basis 99.999%, Sigma Aldrich
- KBr, p.a., ACS, MERCK KGaA
- $NaBH_4$, Alfa Aesar
- Aniline, ACS ≥ 99.5%, Sigma Aldrich
- Ammonium persulfate, APS, Merck
- CABOT Vulcan XC72R (Carbon Black), GP-3820, CAS No. 1333-86-4, Cabot Corporation
- Ultrapure H_2O 18 MΩ, Barnstead Nanopure Water Purification System
- 2-Propanol ASC ≥ 99.8%, Sigma Aldrich
- $HClO_4$ acid concentrate 0.1 mol for 1 l standard solution, Sigma Aldrich (Fixanal, Fluka® Analytical)
- H_2SO_4, 96% Ultrapur., Merck
- Pt/C, Pt nominally 50% on carbon black, Alfa Aesar
- $Pt_{22.5}Co/C$, 30wt% Pt-Co loading, Sigma Aldrich
- Alumina suspension, 0.05 µm, by MasterPrep Bühler
- Nitrogen, 5.0, Air Liquide
- Oxygen, 4.5, Air Liquide

- Hydrogen, 5.0, Air Liquide

3.1.2 Instruments and Equipment

- Reference 600^{TM} Potentiostat/Galvanostat/ZRA, GAMRY Instruments
- Rotating electrode RDE710, GAMRY Instruments
- RDE: ring disk electrode (glassy carbon area 0.196 cm^2), Model AFE5T050GC, Pine Research Instrumentation
- RHE: reversible hydrogen electrode (gaskatel HydroFlex), Gaskatel Gesellschaft für Gassysteme durch Katalyse und Elektrochemie mbH
- Counter electrode: platinized titanium rod, Bank Elektronik – Intelligent controls GmbH
- Julabo, model MC, class: III, Julabo Labortechniken GmbH
- Ultrasonic bath Bandelin Sonorex, BANDELIN electronic GmbH & Co. KG
- Ultrasonic processor UP400S, Hielscher Ultrasound Technology
- Scale: Sartorius BP 110S max. 110 g, Sartorius AG
- Magnetic stirrer: Heidolph MR Hei-Tech, Heidolph Instruments GmbH & Co. KG
- Drying oven: DRY-line, VWR#
- Centrifuge: Labofuge 400, Heraeus
- Lab furnace: Jumo Dicon 501, Elsklo
- Pipette, 1000 µl, pipet4u ® Performance, AHN Biotechnology GmbH
- Pipette, 2-20 µl, pipet4u ® Performance, AHN Biotechnology GmbH
- Pipette tip: 1000 µl, PE, Eppendorf AG

3.1.3 Software

- Gamry Framework Version 6.25, Gamry Instruments
- Gamry Echem Analyst, Gamry Instruments
- My Gamry Data, Gamry Instruments
- Microsoft Office Excel 2010, Microsoft
- MagicPlot Pro

3.2 Catalyst Preparation

Two different methods for the functionalisation of catalysts with PANI were performed. First, commercial Pt_{50}/C and $Pt_{22.5}Co$/C and in-house $Pt_{30}Co$/C catalysts were functionalised with 20 wt% PANI similarly to the supporting information of Chen et al.[35] Additionally, in the second method Vulcan XC72R was functionalised with PANI. Pt NPs were then deposited on the PANI decorated Vulcan XC72R. The indices on the catalyst' names indicate the wt% of Pt.

Table 3 summarizes the catalysts functionalised with PANI.

Table 3: Table of PANI-functionalised catalysts with Pt and PANI contents.

Catalyst	*wt% Pt*	*wt% PANI*	*Method*
Pt_{50}/@$PANI_{20}$	50	20	1
$Pt_{22.5}Co$/C@$PANI_{20}$	22.5	20	1
$Pt_{30}Co$/C@$PANI_{20}$	30	20	1
C@$PANI_{20}$+Pt_{50}	50	20	2
C@$PANI_{20}$+Pt_{20}	20	20	2

3.2.1 PANI Functionalisation

The oxidative polymerisation of aniline according to Chen et al.[5] was performed in an ice bath.

Method 1:

For the first method, a 250 mL round flask was charged with 50 mL 0.5 M H_2SO_4 aqueous solution and. Catalyst was added and the mixture stirred ultrasonically for 30 min. Aniline monomer (20 wt% adjusted to the Pt content of the catalyst) was added and the mixture stirred ultrasonically for 5 h at room temperature. Next, the mixture was cooled in an ice bath. APS dissolved in 20 mL 0.5 M H_2SO_4 aqueous solution was cooled in an ice bath and added to the mixture. The ratio of $n_{aniline}$: n_{APS} was 1:1. The reaction was conducted at 4 °C overnight. The products were centrifuged three times at 3500 rpm and washed with EtOH and ultrapure H_2O after each round. The obtained black precipitate was dried at 40 °C overnight. This method was used to prepare Pt/C@PANI$_{20}$, Pt_{30}Co/C@PANI$_{20}$ and $Pt_{22.5}$Co/C@PANI$_{20}$.

Method 2:

C@PANI$_{20}$+Pt_{50} and C@PANI$_{20}$+Pt_{20} (Table 3) were prepared according to the second method: A 250 mL round flask was charged with Vulcan XC72R (600 mg) and 50 mL 0.5 M H_2SO_4 aqueous solution. Aniline (1.57 mmol) was added and the mixtures stirred ultrasonically for 45 min and subsequently cooled in an ice bath. APS (1.57 mmol), dissolved in 20 mL 0.5 M H_2SO_4 aqueous solution and cooled in an ice bath, was added dropwise. The polymerisation was carried out at 4 °C overnight. The product was centrifuged at 3500 rpm and washed with EtOH and ultrapure H_2O three times. The precipitate was dried at 40 °C to yield PANI-functionalised Vulcan XC72R (C@PANI$_{20}$) as a black powder.

The deposition of Pt NPs was carried out as follows: A 250 mL round flask was charged with PANI-decorated Vulcan XC72R (666 mg) and 0.5 M H_2SO_4 aqueous solution (50 mL). H_2PtCl_6·6 H_2O (20 wt% and 50 wt% for C@PANI$_{20}$+Pt_{20} and C@PANI$_{20}$+Pt_{50}, respectively) was added and the mixture stirred ultrasonically for 45 min. A freshly prepared $NaBH_4$ ($n_{(NaBH4)}$:$n_{(H2PtCl6·6\ H2O)}$ was 15:1) aqueous solution (20 mL) was added dropwise and the mixture stirred ultrasonically at RT for 2 h. The product was centrifuged at 3500 rpm and washed with ultrapure H_2O three times. The precipitate was dried at 40 °C to yield C@PANI$_{20}$+Pt_{50} and C@PANI$_{20}$+Pt_{20} as a black powder.

3.2.2 Catalyst Synthesis

In-house $Pt_{30}Co/C$ catalyst was prepared according to a method described by *Holade* et al.[36]. The amount of Pt was set to 30 wt%. The ratio of Pt:Co was 1:5.

A 250 mL round flask was charged with $H_2PtCl_6 \cdot 6\ H_2O$ (438 mg, 0.85 mmol), $Co(NO_3)_2 \cdot 6\ H_2O$ (4.074 g, 14.00 mmol) and ultrapure H_2O (50 mL). After complete dissolution of the precursor salts, KBr (2.650 g, 22.267 mmol) was added to the solution. Vulcan XC72R (385 mg) was added and the mixture stirred ultrasonically for 45 min. Next, a freshly prepared aqueous solution of $NaBH_4$ in ultrapure H_2O (20 mL) was added dropwise to the mixture and stirred ultrasonically for 2 h. The product was centrifuged at 3500 rpm and the resulting precipitate leached in 10 vol% H_2SO_4 aqueous solution for 30 min. Next, the product was centrifuged at 3500 rpm and washed three times with ultrapure water. After drying at 40 °C, the black residue was heat-treated in a N_2 atmosphere (30-240 °C with a heating rate of 5 °C/min and then held at 240 °C for 45 min) to yield $Pt_{30}Co/C$ as a black powder.

3.3 Ex-Situ Characterisation via RDE

RDE and ORR measurements were performed at 30 °C. All glassware was cleaned by boiling in ultrapure H_2O. The glassy carbon electrode was polished with 0.05 µm alumina suspension and washed with ultrapure H_2O.

The standard three-electrode setup (see Figure 8) consisted of a commercial glassy carbon electrode with 5 mm diameter (area 0.196 cm^2) as WE, a platinised titanium rod as CE and a reversible hydrogen electrode (RHE) as reference electrode. All potentials stated are referenced against the RHE. As electrolyte 0.1 M $HClO_4$ aqueous solution was used. Before and during each CV measurement the electrolyte was purged with N_2 and with O_2 for the ORR polarisation curves to ensure continuous saturation of the electrolyte with the gases.

For the preparation of the catalyst inks, a carefully weighed amount of catalyst was dispersed in 3 mL of a mixture of IPA/H_2O (7:3) using an ultrasonic bath to ensure homogeneous dispersion. A total of amount 10 µL of the ink (2x5 µL) was applied on the glassy carbon

electrode and dried by rotating the electrode at 700 rpm to ensure a thin film of catalyst. The Pt-loading was set to 28 µg cm^{-2}.

Before recording CV and ORR measurements, the catalyst was subjected to potentiodynamic cycling between 0.05-1.10 V with 50 mV s^{-1} in inert electrolyte until a stable potential was reached. These cycles are a mean to rid the catalyst of any potential impurities. Next, three cycles between 0.01-1.10 V are recorded with a scan rate of 10 mV s^{-1} in inert electrolyte for the analysis of the catalyst. Thereafter the electrolyte was purged with O_2 and three cycles recorded between 0.01-1.10 V with a scan rate of 10 mV s^{-1} at different rotation speeds (400, 600, 900, 1200, 1600, 2000 rpm) for determination of the ORR activity.

Additionally, CV and ORR curves were recorded analogously in 0.1 M $HClO_4$ aqueous solution containing 1 mM and 5 mM H_3PO_4 to investigate the degree of catalyst poisoning by phosphate ions. The parameters for all performed ex-situ measurements are listed in Table 4.

Table 4: Parameters for ex-situ measurements.

	Lower vertex vs. RHE/ V	*Upper vertex vs. RHE/ V*	*Scan speed/ mV/s*	*Rotation speed / rpm*	*No. of cycles*
Cleaning	0.05	1.10	50	-	80
CV	0.05	1.10	50	-	3
ORR	0.05	1.10	50	400, 600, 900, 1200, 1600, 2000	3

3.4 Preparation of PANI-Decorated GDEs

For the single cell *in-situ* measurements, pre-prepared gas diffusion electrodes (GDEs) with a known Pt loading were provided by the Elcore® GmbH. With the objective to develop a simple,

quick and inexpensive method for improving both the durability and the catalytic activity of the electrodes, PANI-functionalisation was carried out on these GDEs.

For the functionalisation of the GDEs with PANI, the previously described method from Chen et al.[35] was modified to fit the functionalisation of catalysts on the pre-prepared electrodes.

The electrodes had an area of 293.7 cm^2 and featured Pt loadings of 1.25 mg cm^{-2} and a ratio of catalyst to carbon support of 1:1. For the deposition of 20 wt% PANI on the GDEs, a glass vessel with the appropriate dimensions for the electrode was charged with 175 mL 0.5 M H_2SO_4 aqueous solution and 60 mL IPA. The electrode was submerged in the solution and aniline, dissolved in 25 mL 0.5 M H_2SO_4 aqueous solution, was added to the solution. The vessel was cooled in an ice bath. APS ($n_{Aniline}$:n_{APS} 1:1) was dissolved in 25 mL 0.5 M H_2SO_4 aqueous solution, the solution cooled in an ice bath and added to the reaction vessel. The polymerisation was conducted in an ice bath overnight. Next, the electrodes were washed with ultrapure H_2O and EtOH. Finally, the electrodes were dried at room temperature overnight.

3.5 In-Situ Characterisation of Pt/C@$PANI_{20}$

The PANI decorated GDLs were manufactured into electrodes with a geometric area of 87 cm^2. MEAs were manufactured using the PANI decorated electrodes as the cathode and non-decorated electrodes as the anode (1.25 mg/cm^2 Pt loading). The MEAs were tested in a single cell at a temperature of 160 °C with H_2 or reformate gas for the anode and O_2 for the cathode. The stoichiometries of the gases were 1.25 for H_2 and reformate H_2 and 2.0 for O_2.

A CV as well as a current-voltage characteristic (UI-curve) was recorded at the begin-of-life (BoL) state of the MEA. Afterwards, a long term test was performed. For the long term test, a constant current of 0.2 A was drawn from the cell and the voltage was recorded. A second CV as well as a second UI-curve was recorded after the long term test at the end-of-life state (EoL) of the MEA.

4 Results and Discussion

In order to investigate the universality of the PANI decoration method presented by *Chen* et al.[5] toward catalysts with improved tolerance towards phosphate poisoning and slower degradation rates, several catalysts were functionalised with the polymer and subjected to RDE measurements. The ECSA losses as well as losses of catalytic activity were calculated at different PA concentrations in the electrolyte for both the non-functionalised and the functionalised catalysts. Table 5 summarizes the catalysts investigated by ex-situ RDE measurements.

Table 5: Summary of the catalysts investigated by RDE.

Catalyst	*Pt content/ %*	*PANI content/ %*
Pt_{50}/C	50	-
$Pt_{50}/C@PANI_{20}$	50	20
$Pt_{22.5}Co/C$	22.5	-
$Pt_{22.5}Co/C@PANI_{20}$	22.5	20
$Pt_{30}Co/C$	30	-
$Pt_{30}Co/C@PANI_{20}$	30	20
$C@PANI_{20}+Pt_{50}$	50	20
$C@PANI_{20}+Pt_{20}$	20	20

Additionally, GDEs provided by the Elcore GmbH with Pt-loading were functionalised with PANI and tested by the Elcore GmbH.

In the following sections, the average results of 3 RDE measurements, ORR and CV, are presented and discussed. Important parameters from these measurements such as the ECSA, MA and SCD are presented. The ORR polarisation curves are compared at a rotation rate of

1600 rpm in pure electrolyte and in PA containing electrolyte (1 mM and 5 mM). All voltages are given versus the RHE and corrected for the ohmic resistance of the electrolyte. Levich analysis for the determination of the number of electrons transferred during the reaction was carried out.

4.1 Pt_{50}/C@$PANI_{20}$

4.1.1 Investigation of PA induced ECSA loss

Figure 11 illustrates the CV of a commercial Pt_{50}/C catalyst. The graph corresponds to the typical shape of a Pt based catalyst. Three regions can be assigned to the CV. The region corresponding to ad- and desorption of H_2 (0.05 - 0.4 V), the double layer region (0.4 - 0.6 V) and the region of Pt oxidation and OH-adsorption (0.6 - 1.1 V).[12] Upon introduction of H_3PO_4 into the electrolyte, the curves shape is changed at various points. The sharp peak at 0.13 V of the curve recorded in pure electrolyte decreases in intensity after the introduction of H_3PO_4. However, the curve gains a sharp peak at 0.25 V after introduction of the acid. These two signals are attributed to the Pt(110) and Pt(111) faces, respectively.[12] The sharpening of the latter signal is assumed to be caused by phosphates adsorption on steps on the Pt-surface.[12] The ECSA decreases due to the adsorption of phosphates on the catalyst's surface, by 19% and 29% in1 mM and 5 mM H_3PO_4, respectively.

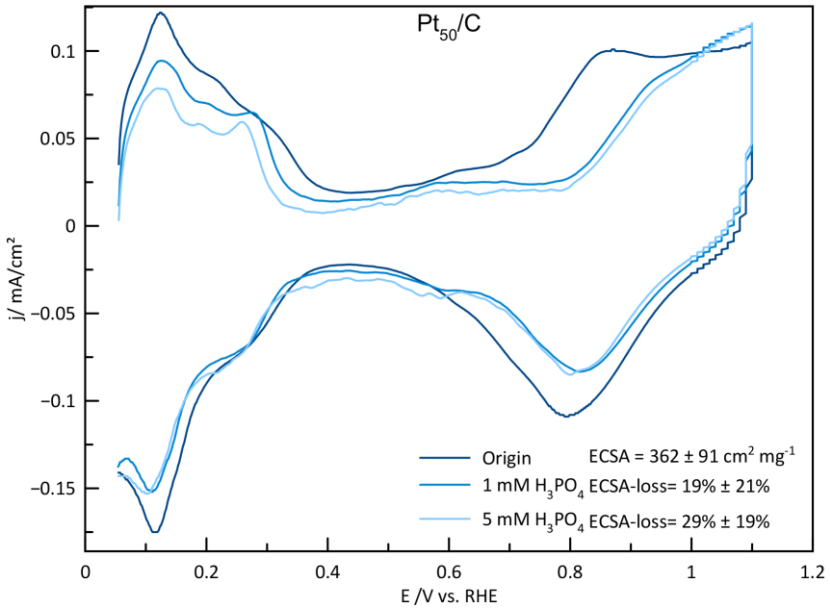

Figure 11: CVs of Pt_{50}/C in 0.1 M $HClO_4$ with 0 mM, 1 mM and 5 mM H_3PO_4, (average of 3 measurements).

The peak corresponding to OH-adsorption and Pt-oxidation (0.8 – 1.0 V) is shifted toward higher potentials, indicating competitive interactions of phosphates with the catalyst surface.[12]

Figure 12 shows the CVs of $Pt_{50}/C@PANI_{20}$. The same phenomena of shifted signals as in Figure 11 can be observed. The main difference between $Pt_{50}/C@PANI_{20}$ and Pt_{50}/C occurs after introduction of H_3PO_4 to the electrolyte. Pt_{50}/C shows an ECSA-loss of 19-29% whereas $Pt_{50}/C@PANI_{20}$ only loses 7-19% of its original ECSA in PA containing electrolyte.

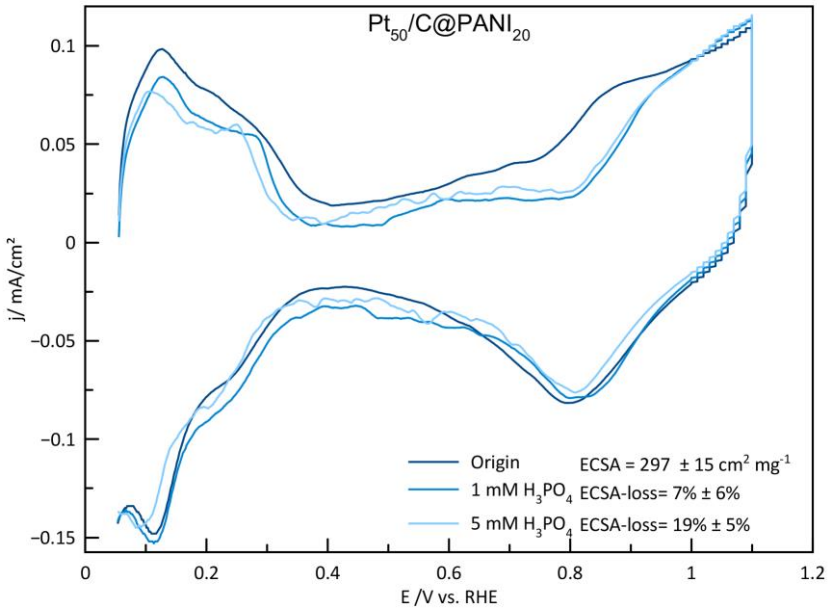

Figure 12: CVs of $Pt_{50}/C@PANI_{20}$ in 0.1 M $HClO_4$ with 0 mM, 1 mM and 5 mM H_3PO_4, (average of 3 measurements).

4.1.2 Catalytic activity

Figure 13 depicts the ORR activities of Pt_{50}/C and $Pt_{50}/C@PANI_{20}$ in 0 mM, 1 mM and 5 mM H_3PO_4 containing electrolyte. Due to the aforementioned competitive adsorption of phosphates on the active sites of the catalyst, the onset potential of the ORR is shifted towards negative potentials for both catalysts upon exposure to PA. While $Pt_{50}/C@PANI_{20}$ exhibits slightly higher onset potentials than Pt_{50}/C in 0 mM and in 1 mM H_3PO_4, Pt_{50}/C catalyst outperforms $Pt_{50}/C@PANI_{20}$ in 5 mM H_3PO_4. Although $Pt_{50}/C@PANI_{20}$ features a lower ECSA, its kinetic limited current of 5.5 mA/cm^2 between 0.2-0.5 V is well above that of Pt_{50}/C which is about 4.8 mA/cm^2.

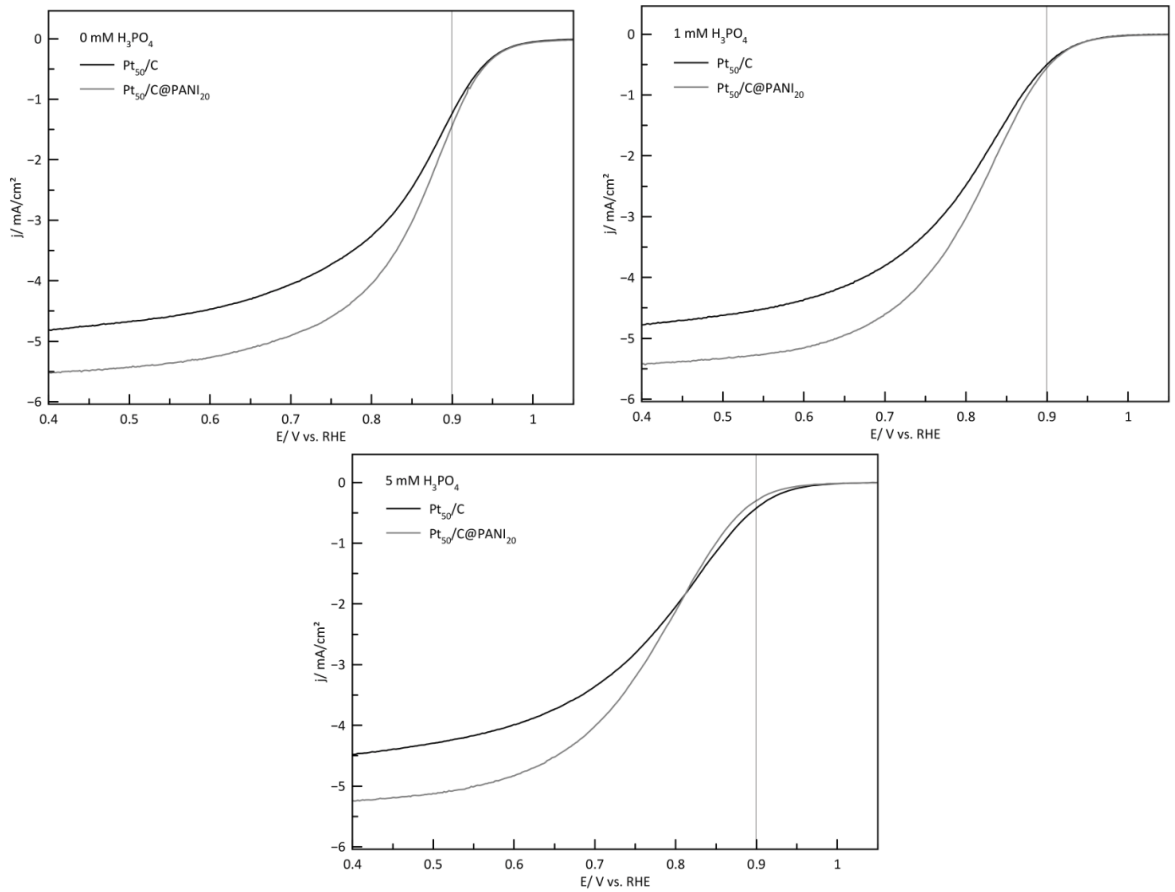

Figure 13: ORR activities at 1600 rpm of Pt_{50}/C and $Pt_{50}/C@PANI_{20}$ in 0 mM, 1 mM and 5 mM H_3PO_4, (average of 3 measurements).

Figure 14 shows the mass activity as well as the specific current density of both catalysts before and after exposure to PA. As with the ORR activity, $Pt_{50}/C@PANI_{20}$ exhibits higher MA and SCD with 0.054 ± 0.012 A/mg and 0.160 ± 0.016 mA/cm^2 in pure electrolyte, respectively. However, after exposure to 5 mM H_3PO_4, $Pt_{50}/C@PANI_{20}$ produced 0.013 ± 0.001 A/mg and 0.051 ± 0.015 mA/cm^2 while Pt_{50}/C developed 0.020 ± 0.004 A/mg and 0.070 ± 0.016 mA/cm^2. As the thickness of the PANI layer is stated as the most significant factor for the effectiveness of PANI-decorated catalysts,[5] it is assumed that a 20wt% PANI loading is too little for this specific catalyst and thus creates a too shallow shell around the Pt/C particles in order to effectively protect the catalyst against PA adsorption.

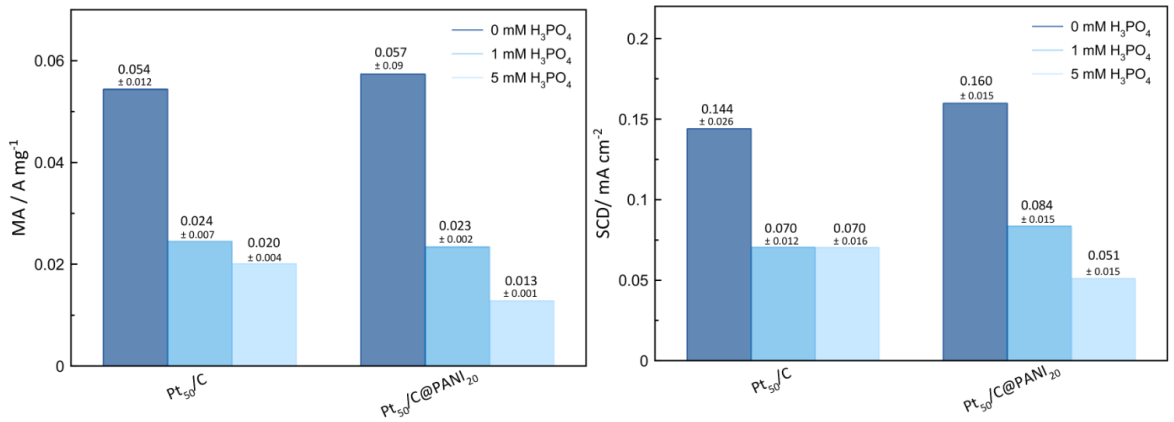

Figure 14: MAs and SCDs of Pt_{50}/C and $Pt_{50}/C@PANI_{20}$ in 0 mM, 1 mM and 5 mM H_3PO_4 at 1600 rpm, (average of 3 measurements).

4.2 In-house $Pt_{30}Co@PANI_{20}$ and commercial $Pt_{22.5}Co@PANI_{20}$

4.2.1 Investigation of PA induced ECSA loss

Figure 15 illustrates the CV in inert electrolyte of an in-house $Pt_{30}Co/C$ catalyst. Its initial ECSA (242 cm^2/mg) is lower than of the Pt_{50}/C catalyst and $Pt_{50}/C@PANI_{20}$. After introduction of 1 mM H_3PO_4 and 5 mM H_3PO_4 the ECSA-losses of $Pt_{30}Co/C$ are 26 % and 44 %, respectively. The change in the signal sharpness at 0.25 V and 0.8-1.0 V after introduction of PA are attributed to the competitive adsorption of the phosphate ions on the potential-induced surface steps of the Pt-surface and the thus hindered Pt oxidation.[12]

The CVs of $Pt_{30}Co/C@PANI_{20}$ (Figure 16) show a similar behaviour. The ECSAs of both $Pt_{30}Co/C$ and $Pt_{30}Co$ /$C@PANI_{20}$ are almost the same in pure 0.1 M $HClO_4$. However, in 5 mM PA, $Pt_{30}Co/C$ loses 44% of its original ECSA whereas $Pt_{30}Co$ @$PANI_{20}$ only loses 36%. This slight improvement in the resistivity towards phosphate poisoning is attributed to the PANI-coating around the catalyst particles. $Pt_{30}Co$ /$C@PANI_{20}$ (Figure 16) also exhibits two slight peaks between 0.4 and 0.8 V which are caused by the oxidation and reduction of the $PANI_{20}$, respectively.

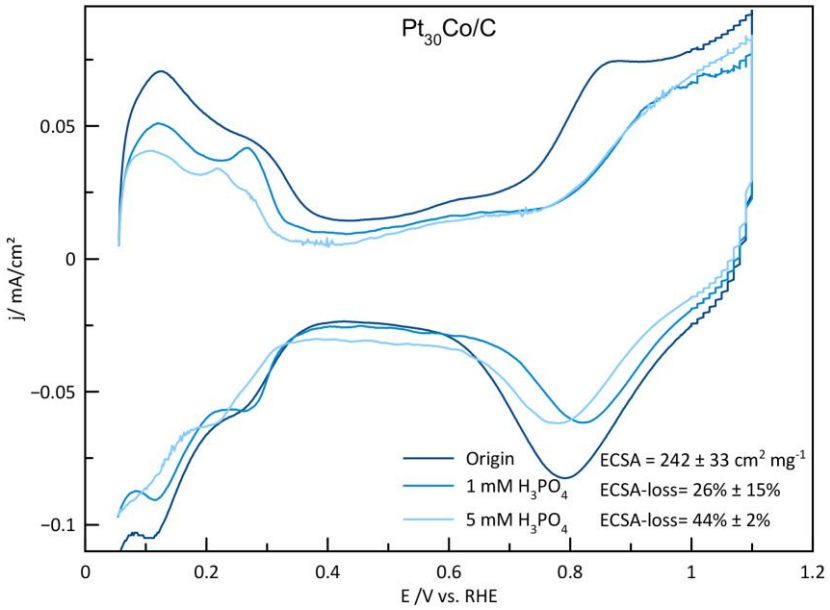

Figure 15: CV of $Pt_{30}Co/C$ in 0.1 M $HClO_4$ with 0 mM, 1 mM and 5 mM H_3PO_4, (average of 3 measurements).

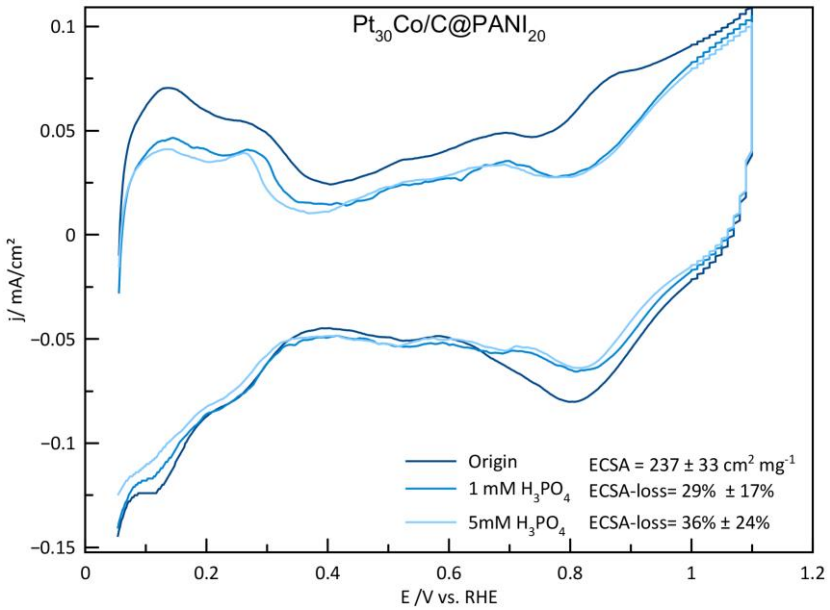

Figure 16: CV of $Pt_{30}Co$ /C@$PANI_{20}$ in 0.1 M $HClO_4$ with 0 mM, 1 mM and 5 mM H_3PO_4, (average of 3 measurements).

The CV in inert electrolyte of a commercial $Pt_{22.5}Co/C$ and $Pt_{22.5}Co/C@PANI_{20}$ are shown in Figure 17 and Figure 18.

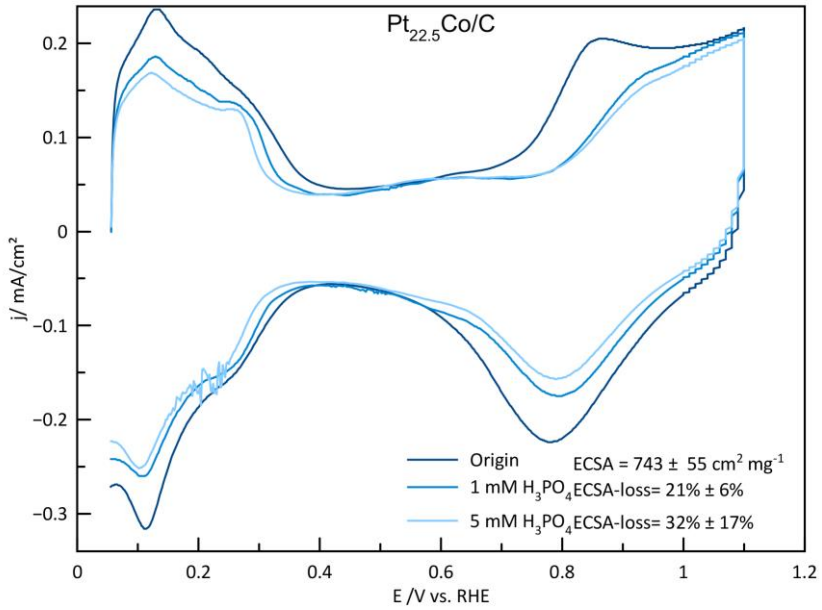

Figure 17: CV of $Pt_{22.5}Co/C$ in 0.1 M $HClO_4$ with 0 mM, 1 mM and 5 mM H_3PO_4, (average of 3 measurements).

The CV of $Pt_{22.5}Co/C$ shows a large initial ECSA of 743 cm^2/mg and defined peaks. After addition of 1 mM and 5 mM PA, the ECSA-loss was 21% and 32%, respectively. In comparison to Pt_{50}/C, which has almost twice the Pt content of $Pt_{22.5}Co/C$, the losses of catalyst surface are very similar with $Pt_{22.5}Co/C$ suffering only a 2-3 % higher loss. However, the initial ECSA of $Pt_{22.5}Co/C$ is more than twice as high than that of Pt_{50}/C. The peak sharpening and shifting phenomena are equally detailed as for Pt_{50}/C and $Pt_{50}/C@PANI_{20}$ catalysts in PA. After decoration with $PANI_{20}$, $Pt_{22.5}Co/C@PANI_{20}$ only exhibited an initial ECSA of 447 cm^2/mg, almost 300 cm^2/mg less than $Pt_{22.5}Co/C$. ECSA losses for $Pt_{22.5}Co/C@PANI_{20}$ are also very similar to that of $Pt_{22.5}Co/C$, that of $Pt_{22.5}Co/C@PANI_{20}$ being only 2-4 % less.

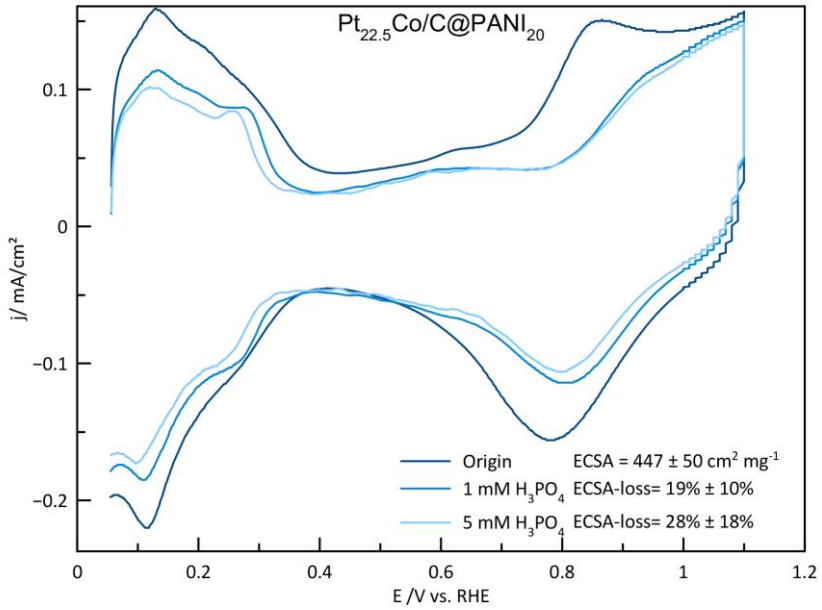

Figure 18: CV of $Pt_{22.5}Co/C@PANI_{20}$ in 0.1 M $HClO_4$ with 0 mM, 1 mM and 5 mM H_3PO_4, (average of 3 measurements).

4.2.2 Catalytic Activity

Figure 19 shows the ORR polarisation curves of $Pt_{22.5}Co/C$, $Pt_{22.5}Co/C@PANI_{20}$, $Pt_{30}Co/C$ and $Pt_{30}Co/C@PANI_{20}$ and Pt_{50}/C, which is added as reference.

Figure 19 illustrates that $Pt_{30}Co/C@PANI_{20}$ significantly improves upon $Pt_{30}Co/C$ in regard to ORR activity. $Pt_{30}Co/C@PANI_{20}$ has a higher onset potential as well as a higher diffusion limited current than $Pt_{30}Co/C$. $Pt_{30}Co/C@PANI_{20}$ features much higher current densities at 0.9 V than pure $Pt_{30}Co/C$. The diffusion limited current (0.2 V-0.4 V) also improved notably after decoration with PANI. $Pt_{30}Co/C$ exhibits the highest diffusion limited current density of all examined Pt-Co/C catalysts. The current densities of Pt_{50}/C and $Pt_{30}Co/C@PANI_{20}$ are almost the same at 0.9 V for each PA concentration. Both $Pt_{22.5}Co/C$ and $Pt_{22.5}Co/C@PANI_{20}$ show higher current densities than the commercial Pt_{50}/C. Contrary to expectations, the functionalisation of $Pt_{22.5}Co/C$ with PANI did not lead to an improvement in its activity towards the ORR. This is indicated by the lower current densities at 0.9 V of $Pt_{22.5}Co/C@PANI_{20}$ compared to that of $Pt_{22.5}Co/C$. It is assumed that the PANI-content is not adjusted optimally and the PANI layer is insufficient to protect the catalyst against PA adsorption.

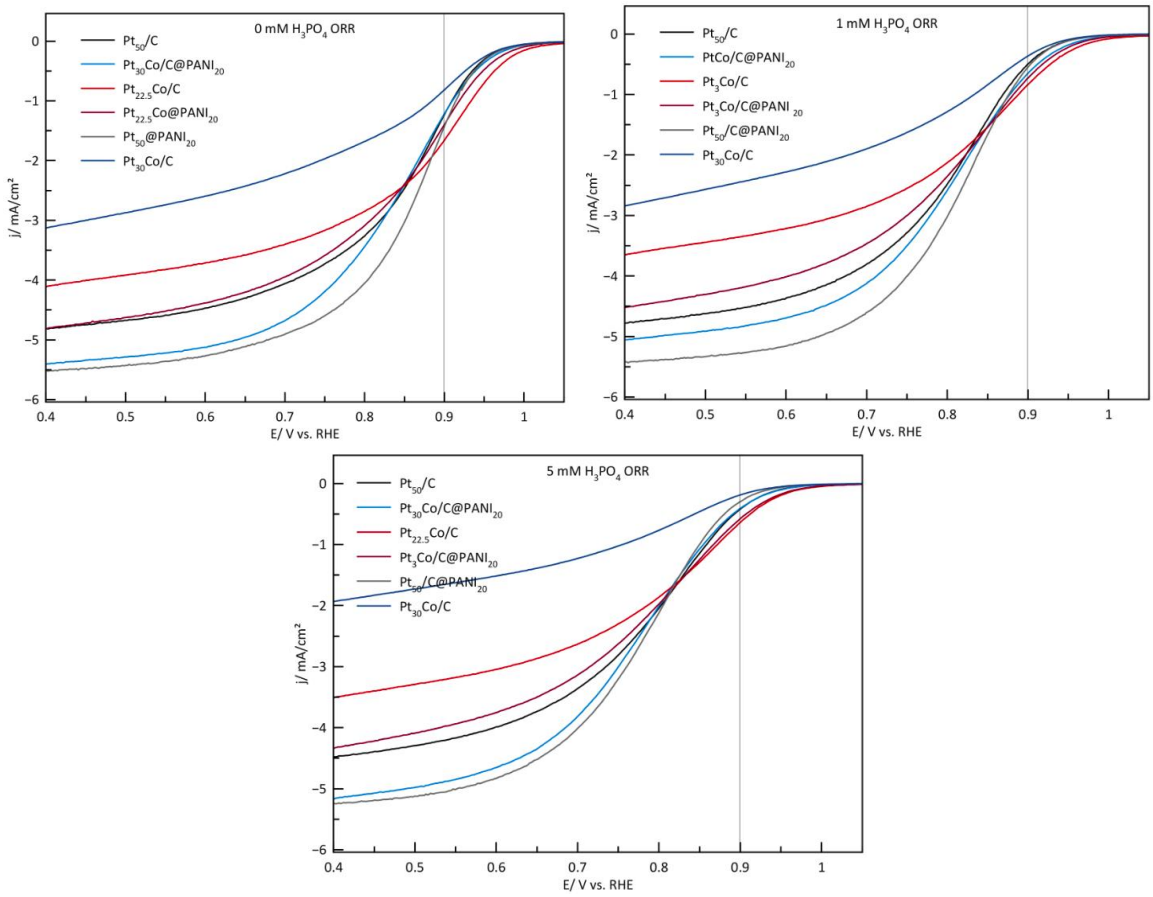

Figure 19: ORR activities of $Pt_{30}Co/C$, $Pt_{30}Co/C@PANI_{20}$, $Pt_{22.5}Co/C$ and $Pt_{22.5}Co/C@PANI_{20}$ in 0 mM, 1 mM and 5 mM H_3PO_4, (average of 3 measurements).

The MA and SCD of $Pt_{30}Co/C$, $Pt_{30}Co/C@PANI_{20}$, $Pt_{22.5}Co/C$ and $Pt_{22.5}Co/C@PANI_{20}$ in different PA concentrations are shown in Figure 20.

Of all catalysts, $Pt_{22.5}Co/C$ shows the highest MA of 0.069 ± 0.020 A/mg in pure electrolyte. Also in 1 mM and 5 mM H_3PO_4 containing electrolyte it exhibits the highest MAs of 0.040 ± 0.020 and 0.026 ± 0.015 A/mg, respectively. After functionalisation with PANI, the MA of $Pt_{22.5}Co/C@PANI_{20}$ in pure electrolyte dropped to 0.058 ± 0.01 A/mg which is still higher than that of $Pt_{50}C$ and $Pt_{50}/C@PANI_{20}$ (see Figure 14). The MA of $Pt_{22.5}Co/C@PANI_{20}$ in 1 mM and in 5 mM H_3PO_4 also dropped slightly to 0.032 ± 0.005 and 0.024 ± 0.006 A/mg, respectively, which are the second highest values for the MA of all tested catalysts shown in Figure 20. Apparently, PANI does not improve the catalytic activity of $Pt_{22.5}Co/C$.

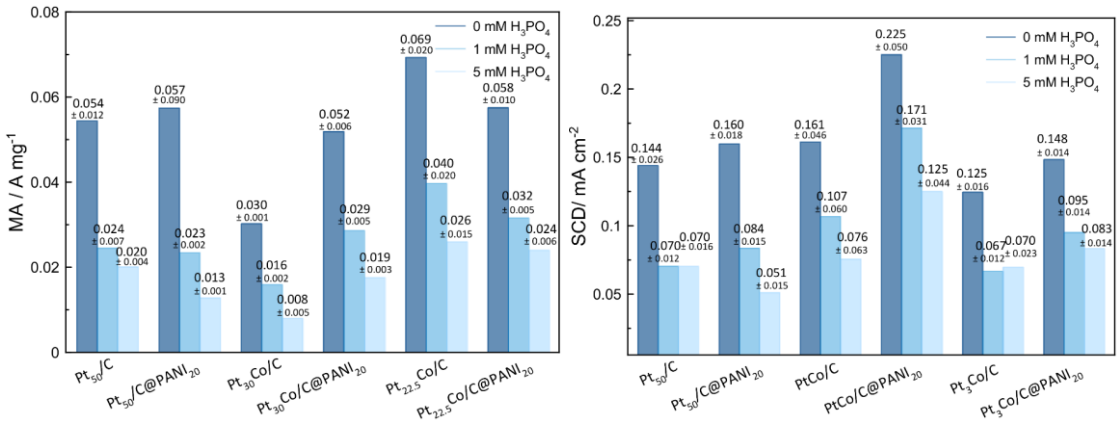

Figure 20: MA and SCD of Pt_{50}/C, Pt_{50}/C@PANI$_{20}$, $Pt_{30}Co$/C, $Pt_{30}Co$/C@PANI$_{20}$, $Pt_{22.5}Co$/C and $Pt_{22.5}Co$/C@PANI$_{20}$ at 0 mM, 1 mM and 5 mM H_3PO_4, (average of 3 measurements).

The in-house $Pt_{30}Co$/C catalyst exhibits the lowest MAs of all catalysts investigated. In pure electrolyte its MA of 0.030 ± 0.001 A/mg is half of that of $Pt_{22.5}Co$/C. In 1 mM and in 5 mM H_3PO_4 the MA of $Pt_{30}Co$/C is 0.016 ± 0.002 A/mg and 0.008 ± 0.005 A/mg, respectively. In contrast to $Pt_{22.5}Co$/C@PANI$_{20}$, which didn't achieve an improvement in the ECSA or the catalytic activity over P_3Co/C, in-house $Pt_{30}Co$/C@PANI$_{20}$ exhibits nearly double the MA at the respective PA concentrations than the in-house $Pt_{30}Co$/C catalyst.

Regarding the SCD, $Pt_{30}Co$/C features the highest values of all non-functionalised catalysts. $Pt_{30}Co$/C@PANI$_{20}$ shows the highest SCD values overall with 0.225 ± 0.050 mA/cm^2 in pure electrolyte and 0.125 ± 0.044 mA/cm^2 in 5 mM H_3PO_4.

Conversely, $Pt_{22.5}Co$/C, which showed the highest MA of all catalysts, features the lowest SCD of all catalysts investigated, showing 0.125 ± 0.016 mA/cm^2 in pure electrolyte and dropping to 0.070 ± 0.023 mA/cm^2 in 5 mM H_3PO_4. $Pt_{22.5}Co$/C@PANI$_{20}$ shows only minor improvements with 0.148 ± 0.014 mA/cm^2 initially and 0.083 ± 0.014 mA/cm^2 in 5 mM H_3PO_4 containing electrolyte.

4.3 C@PANI$_{20}$+Pt$_{20}$ and C@PANI$_{20}$+Pt$_{50}$ Catalysts

4.3.1 Investigation of PA induced ECSA loss

The CV curves in inert electrolyte of C@PANI$_{20}$+Pt$_{20}$ are illustrated in Figure 1. Its initial ECSA was 343 ± 35 cm^2/mg. The ECSA decreases by 18% ± 10% in 1 mM PA and by 22% ± 3% in 5 mM PA. Striking in the CV of this catalyst is the large peak between 0.4 and 0.8 V, which corresponds to the oxidation and reduction of the PANI, completely overshadowing the double-layer region and blending into the Pt-oxidation region.[37]

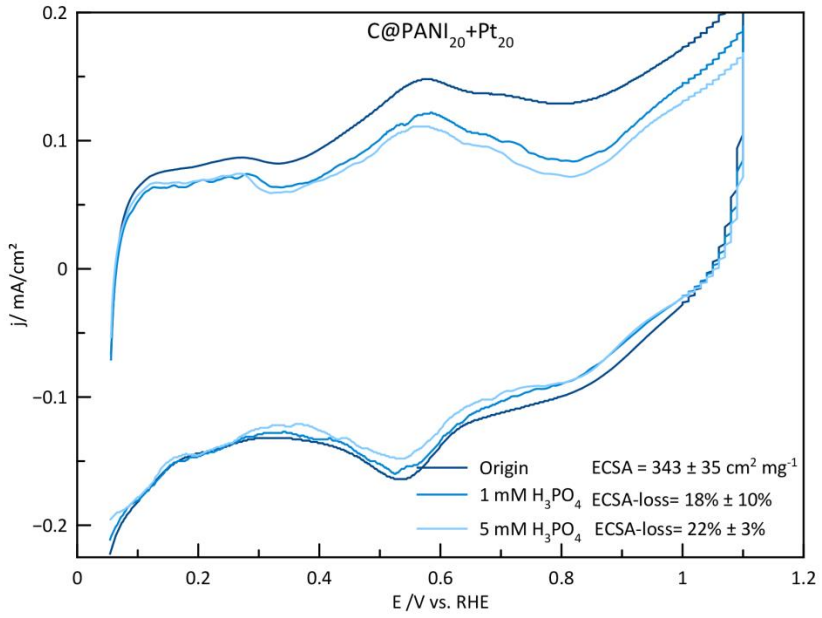

Figure 21: CV of C@PANI$_{20}$+Pt$_{20}$ in 0.1 M $HClO_4$ with 0 mM, 1 mM and 5 mM H_3PO_4, (average of 3 measurements).

In Figure 22 the CV curves of C@PANI$_{20}$+Pt$_{50}$ are depicted. It features the same striking peak between 0.4 and 0.8 V corresponding to PANI oxidation and reduction. While the initial ECSA of C@PANI$_{20}$+Pt$_{50}$ is lower than that of C@PANI$_{20}$+Pt$_{20}$ (277 ± 35 cm^2/mg), the catalyst experiences rather a total increase in the ECSA of 10% ± 9% and 4% ± 2% in 1 mM and in 5 mM H_3PO_4, respectively.

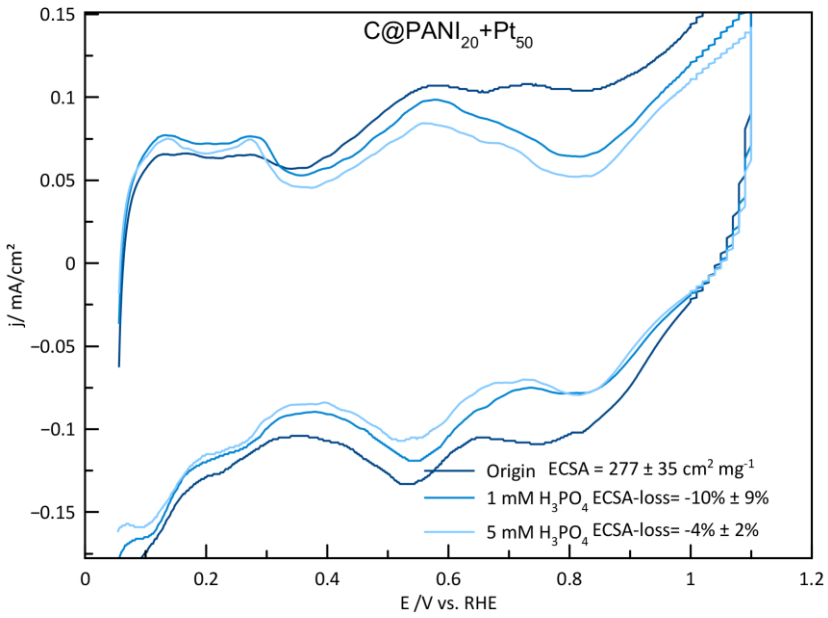

Figure 22: CV of C@PANI$_{20}$+Pt$_{50}$ in 0.1 M $HClO_4$ with 0 mM, 1 mM and 5 mM H_3PO_4, (average of 3 measurements).

4.3.2 Catalytic Activity

Figure 23 shows the ORR polarisation curves of C@PANI$_{20}$+Pt$_{20}$, C@PANI$_{20}$+Pt$_{50}$ as well as of Pt$_{50}$/C. In pure electrolyte, both catalysts Pt$_{50}$/C and C@PANI$_{20}$+Pt$_{50}$ have similar onset potentials, whereby C@PANI$_{20}$+Pt$_{20}$ has the lowest onset potential of all illustrated catalysts. C@PANI$_{20}$+Pt$_{50}$ experiences the least shift of onset potential 1 mM and 5 mM H_3PO_4 and offers the highest current densities at 0.9 V.

Although Pt$_{50}$/C@PANI$_{20}$ and C@PANI$_{20}$+Pt$_{50}$ have identical Pt loadings and PANI contents, their catalytic activity and stability against phosphate poisoning differs drastically. The most likely reason for this might be the different synthesis pathways of the two catalysts. Since in the case of C@PANI$_{20}$+Pt$_{50}$, PANI was deposited on the carbon support before depositing the Pt, the active surface of the precious metal remains free of the PANI, allowing for the precious metal to unfold a high catalytic activity.

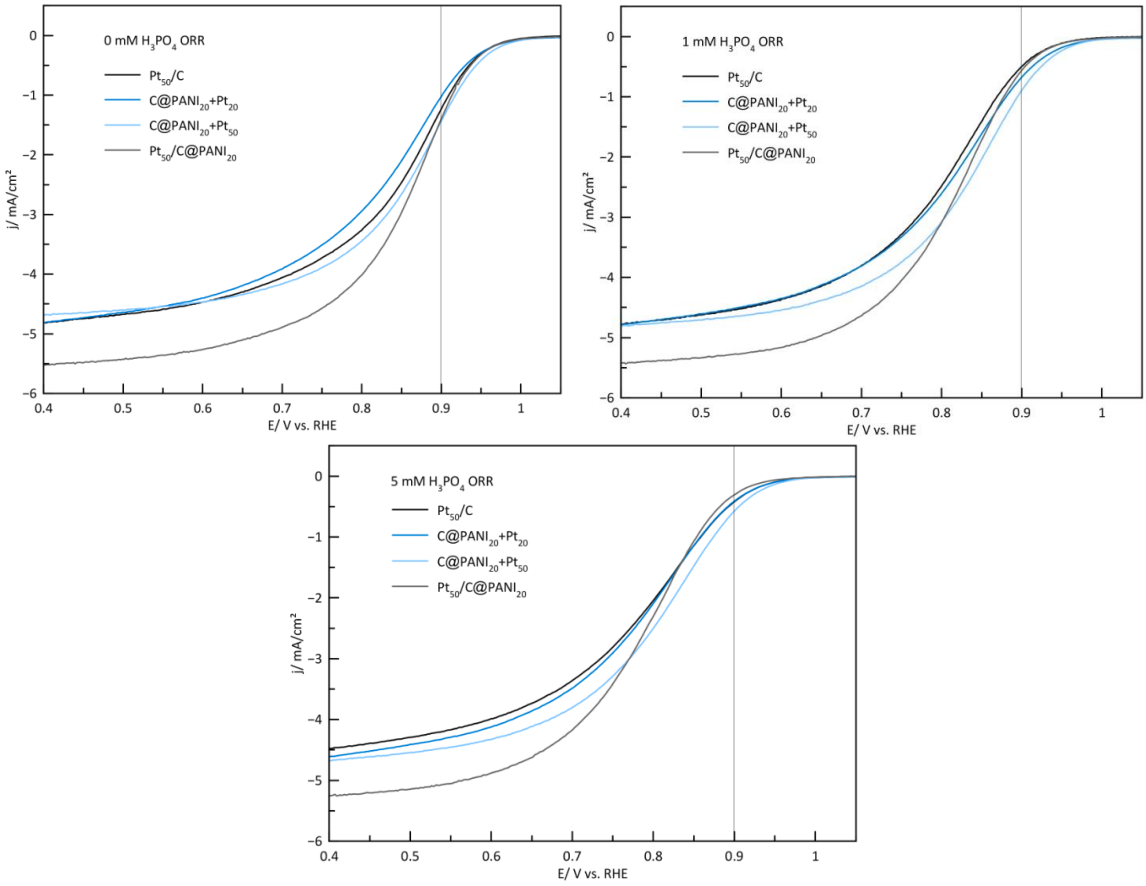

Figure 23: ORR activities of C@PANI$_{20}$+Pt$_{20}$ and C@PANI$_{20}$+Pt$_{50}$ and in 0 mM, 1 mM and 5 mM H_3PO_4, (average of 3 measurements).

Figure 24 depicts the MA and the SCD of C@PANI$_{20}$+Pt$_{20}$ and C@PANI$_{20}$+Pt$_{50}$ as well as that of Pt$_{50}$/C. C@PANI$_{20}$+Pt$_{50}$ offers the highest MA of all catalysts at all PA concentrations. It features far less degradation than Pt$_{50}$/C@PANI$_{20}$ despite equal Pt and PANI loadings and exhibits 0.026 ± 0.005 A/mg in 5 mM H_3PO_4 where Pt$_{50}$/C@PANI$_{20}$ only has 0.013 ± 0.001 A/mg. For C@PANI$_{20}$+Pt$_{20}$, the initial MA is lower than for Pt$_{50}$/C and Pt$_{50}$/C@PANI$_{20}$ at 0.045 A/mg. However, degradation in the presence of phosphates is much lower than for the Pt$_{50}$/C based catalysts. In 1 mM and in 5 mM H_3PO_4, C@PANI$_{20}$+Pt$_{20}$ shows higher MA than both Pt$_{50}$/C and Pt$_{50}$/C@PANI$_{20}$ even though the Pt content of @PANI$_{20}$+Pt$_{20}$ is lower than that of Pt$_{50}$/C and Pt$_{50}$/C@PANI$_{20}$.

From these results it can be assumed that the positive gains resulting from the functionalisation with PANI functionalisation are more pronounced when the functionalisation takes place before the deposition of the catalyst NPs on the support

material. In case of this synthesis pathway, the Pt NPs remain free of PANI while the whole area of the carbon support is protected against PA poisoning.

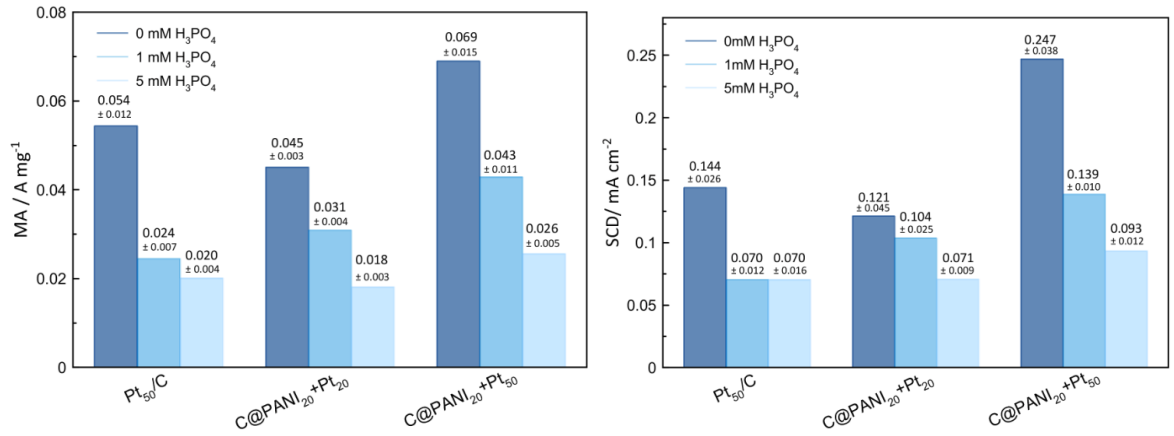

Figure 24: Mass activity C@PANI$_{20}$+Pt$_{20}$ and C@PANI$_{20}$+Pt$_{50}$ as well as Pt$_{50}$/C and Pt$_{50}$/C@PANI$_{20}$ in 0 mM, 1 mM and 5 mM H_3PO_4, (average of 3 measurements).

C@PANI$_{20}$+Pt$_{50}$ possesses the highest initial SCD of all tested catalysts with 0.247 mA/cm^2 and the overall second highest values in 1 mM and in 5 mM H_3PO_4 with 0.139 ± 0.010 mA/cm^2 and 0.093 ± 0.012 mA/cm^2, respectively. C@PANI$_{20}$+Pt$_{20}$ shows a rather low initial SCD of 0.121 ± 0.045 mA/cm^2 but degradation is far less pronounced as for the other catalysts depicted in Figure 20.

4.4 Levich Analysis

To calculate the number of electrons exchanged during the ORR, the Levich equation (Section 2.5, Eq. 2-14) was employed. The square root of the rotation speed $\omega^{1/2}$ is plotted against j_d, which gives a linear relationship with an intersection in the origin. The number of electrons n can be calculated from the slope of the linear plot according to Eq. 2-14. The number of electrons transferred during the ORR n provides information about the mechanism of the ORR. When the value of n is four it can be assumed that only H_2O is produced during the reaction. If the value n is less than four, H_2O_2 is produced during the reaction next to H_2O. In the reaction pathway for the formation of H_2O_2, only two electrons are transferred, resulting in an average electron number that is lower than four.[34]

Figure 25, Figure 26 and Figure 27 illustrate the Levich plots of all analysed catalyst. The figures illustrate that the addition of PA does not alter the mechanism of the reaction as the value for n is similar for every catalyst at all PA concentrations. It also becomes apparent that the functionalisation with PANI does not change the mechanism of the ORR significantly. The only catalyst that shows a change in the value of transferred electrons is $Pt_{30}Co/C$ (see Figure 27). All other catalysts proceed mainly according to the four electron pathway and show a value for n close to four.

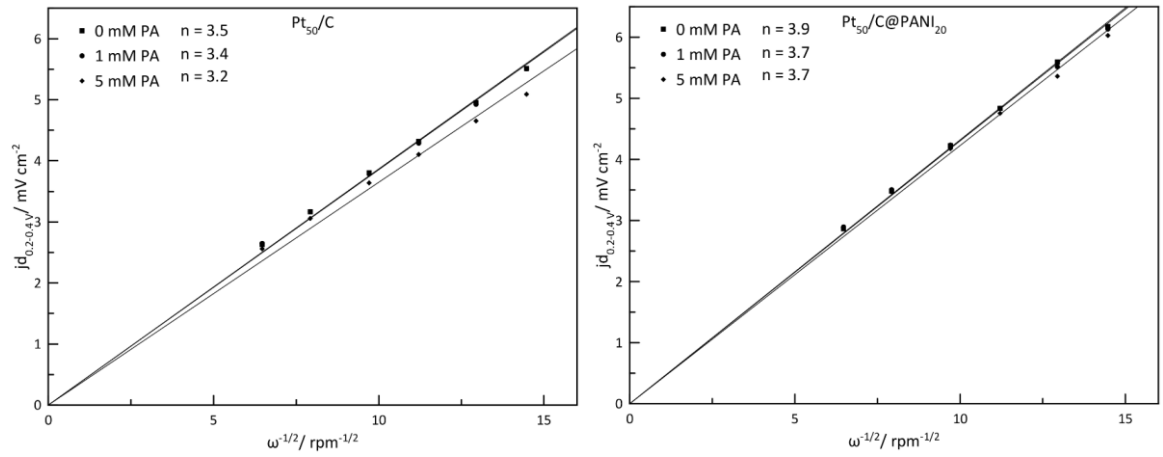

Figure 25: Levich plots of Pt_{50}/C and $Pt_{50}C@PANI_{20}$.

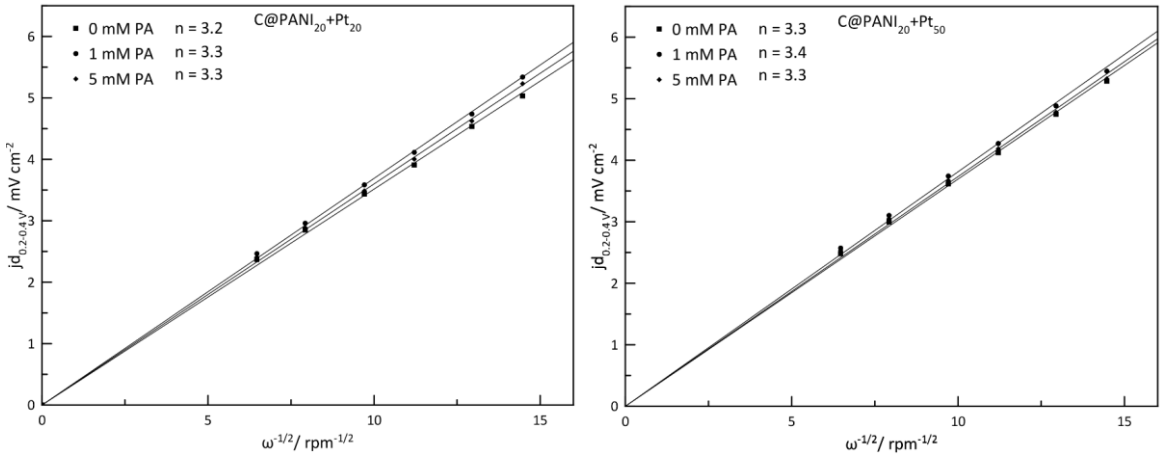

Figure 26: Levich plots of $C@PANI_{20}+Pt_{20}$ and $C@PANI_{20}+Pt_{50}$.

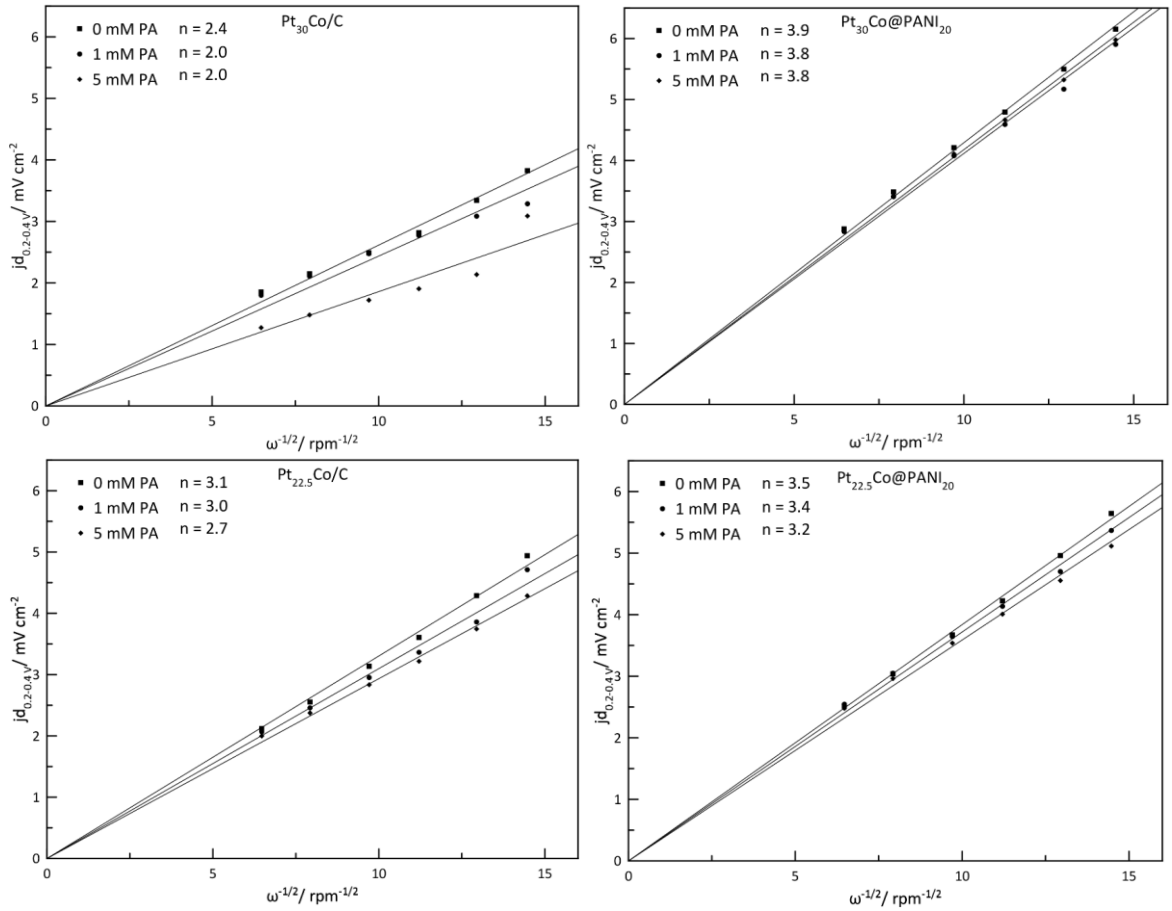

Figure 27: Levich plots of $Pt_{30}Co/C$, $Pt_{30}Co/C@PANI_{20}$, $Pt_{22.5}Co/C@PANI_{20}$ and $Pt_{22.5}Co/C@PANI_{20}$.

4.5 In-Situ Testing of $Pt/C@PANI_{20}$

Three MEAs (PA01, PA02 and PA03) were manufactured by the Elcore GmbH using PANI decorated electrodes on the cathode side. To evaluate the effects of the PANI functionalisation on the CVs and the UI characteristics, a standard non-functionalised electrode with a similar Pt loading was used as a reference.

4.5.1 PA01

Figure 28 illustrates the BoL CV of PA01. At BoL, PA01 showed an ECSA of 129 cm^2/mg which is 6% higher than that of a non-functionalised reference electrode. The raised ECSA indicates that the PANI functionalisation has positively influenced the catalyst on the electrodes.

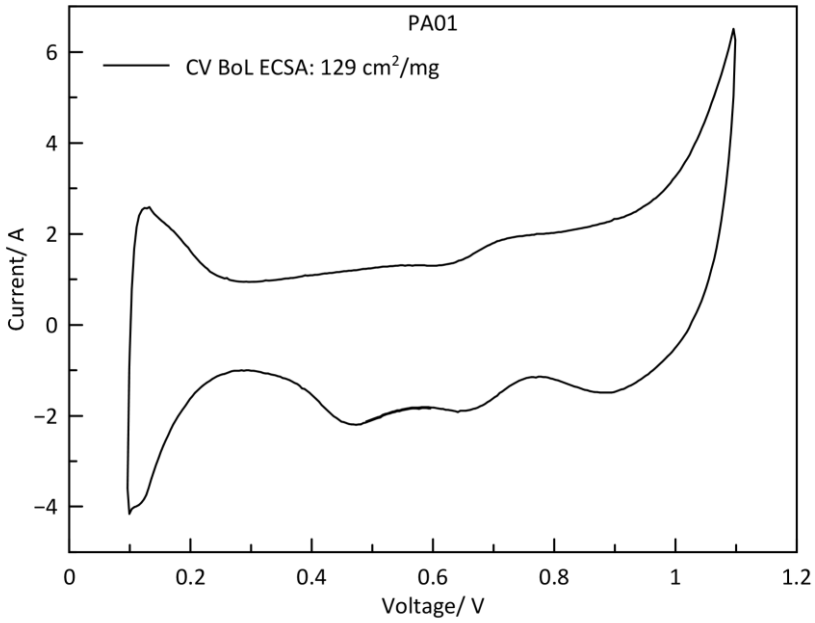

Figure 28: BoL CV of of PA01.

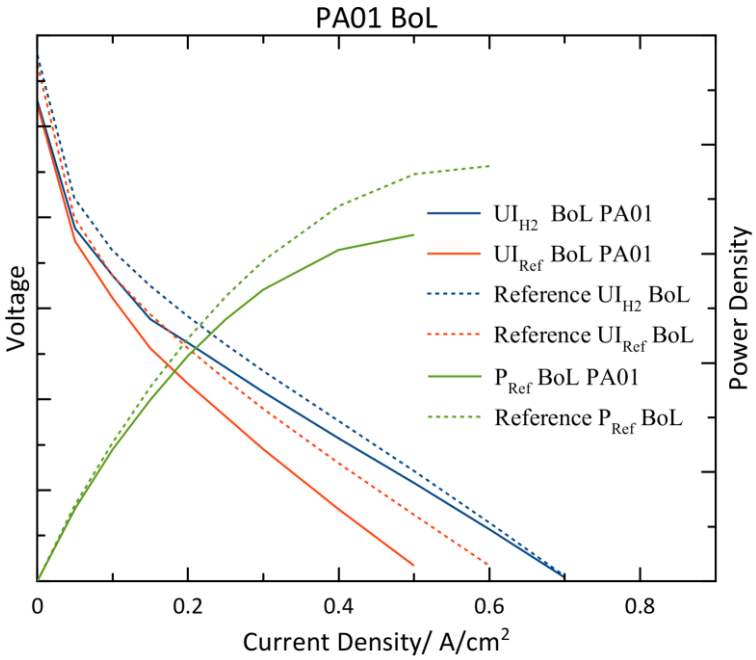

Figure 29: BoL UI characteristic of PA01.

Figure 29 illustrates the BoL UI of PA01. As expected, the UI characteristic of pure H_2 (UI_{H2}) features higher potentials than the UI of reformate H_2 (UI_{Ref}). The BoL open circuit voltage (OCV) of PA01 is lower than that of the reference electrode. The power density (P_{Ref}) of PA01 using reformate H_2 is very similar to that of the reference electrode in the lower potential range.

The first 500 h of the long term test of PA01 are shown in Figure 30. The initial potential of the cell is rather low with 550 mV. After 80 h of operation a stable potential of 600 mV was reached. During the operation of the cell, the mass flow controller (MFC) of H_2 malfunctioned. This caused a constant shortage of H_2 in the cell, resulting in the notable voltage changes which are illustrated in Figure 30. The long term test was prematurely stopped due to the malfunction. However, despite the continuous stress caused by the fluctuating potential and H_2 shortage, the cell showed a stable mean-potential of 600 mV after 800 h of operation.

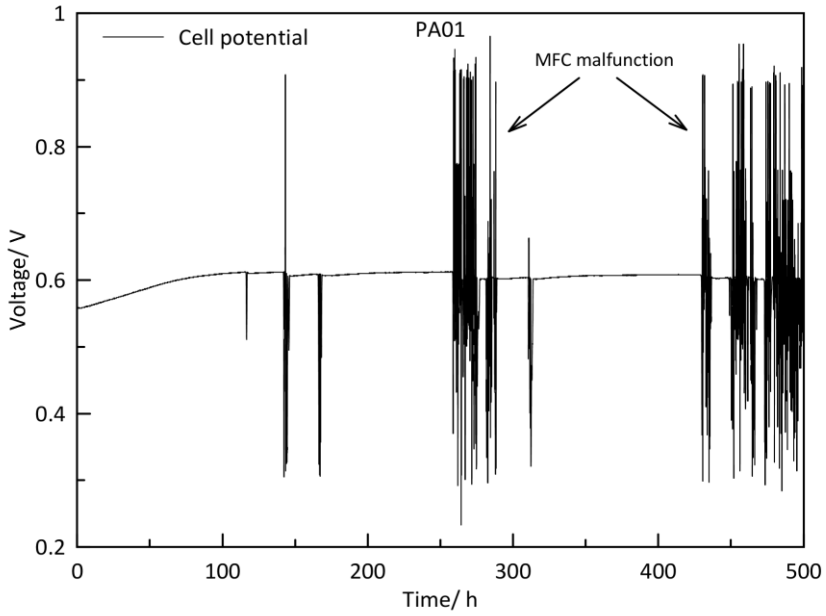

Figure 30: Long term test of PA01 at 160 °C and 0.2 A/cm².

The EoL UI characteristic of PA01 is depicted in Figure 31. Both UI_{Ref} and UI_{H2} of PA01 have shifted to higher potentials despite the long term test (800 h) and the stress caused by the continuous shortage of H_2 in the cell. The non-functionalised reference electrode features lower UI characteristics at EoL conditions than at BoL and offers lower overall potentials than PA01. After 800h of operation, at 0.2 A/cm^2 PA01 improved both its potential and its power density by 3%. On the other hand, after 500 h of operation the potential of the reference electrode dropped by 7% and its power density declined by 90% of its initial value at the same operation point. It is apparent from the data that the PANI functionalisation has a significant positive effect on the stability of the electrodes.

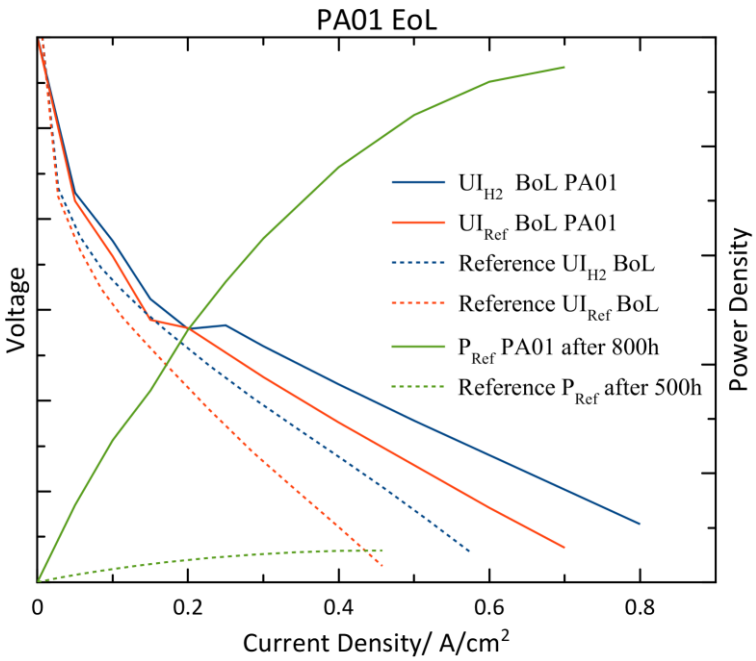

Figure 31: EoL UI characteristic of PA01.

4.5.2 PA02

The BoL UI characteristic is shown in Figure 32. The BoL OCV of PA02 is lower than that of the reference electrode and similar to the BoL OCV of PA01. At BoL PA02 features poor UI_{Ref} and UI_{H2} characteristics and a much lower power density than PA01 and the reference electrode.

The long term test of PA02 is illustrated in Figure 33. PA02 features low potentials during the first 240 h of the test before reaching a stable potential of 630 mV which is over 10 mV more than the reference electrode after the same time of operation. The potential of PA02 is stable at 630 mV for the next 900 h of the long term test. During this time, the electrode has a significantly low degradation rate of 0.14% per 100 h. After 1200 h of operation, the test was paused and resumed 10 days later which resulted in a potential drop to 615 mV. After the same time of operation, the reference electrode exhibited a potential of 590 mV. Overall, PA02 has a significantly lower degradation rate than the non-functionalised electrode.

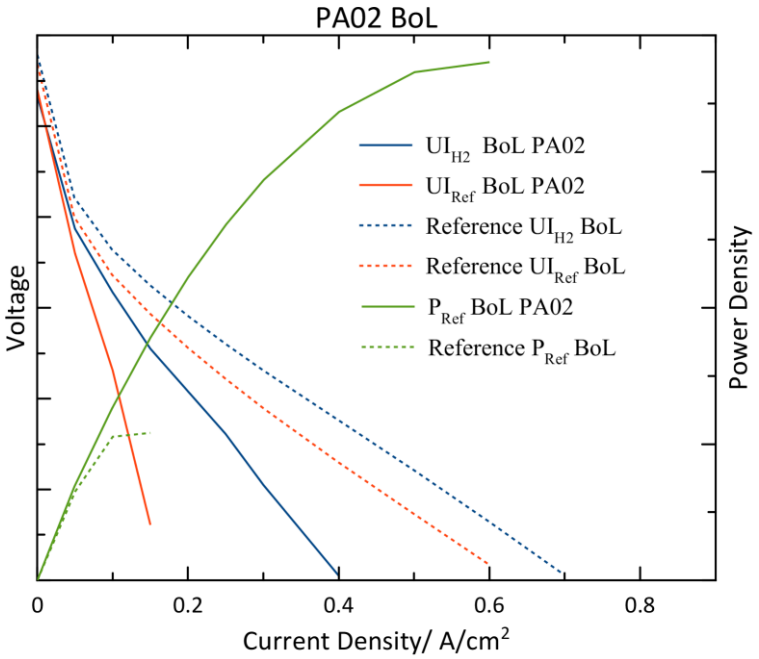

Figure 32: BoL UI characteristic of PA02.

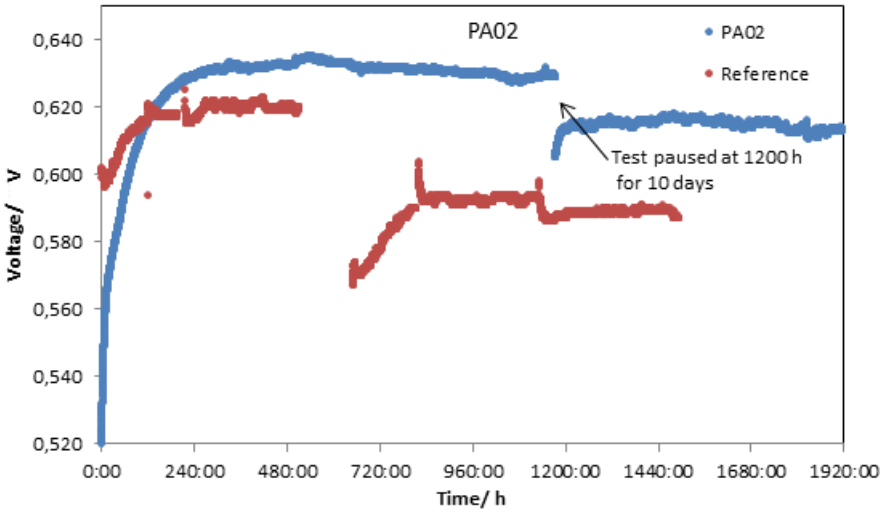

Figure 33: Long term test of PA02 at 160 °C and 0.2 A/cm².

Figure 34 depicts the EoL UI characteristics of PA02. The characteristics are similar to that of PA01 in the EoL state. The P_{Ref} of PA02 at EoL is much higher than at BoL. Both the EoL UI_{Ref} and the EoL UI_{H2} of PA02 feature higher potentials than the reference electrode, even though the reference electrode was only operated for 1300 h and PA02 was operated for 2000 h. After 1200 h of operation, at 0.2 A/cm² PA02 improved its potential and its power density by 20% over its initial values at BoL. After 1300 h, the reference electrode lost 12% of its initial potential and 91% of its initial power density at the same operation point of 0.2 A/cm².

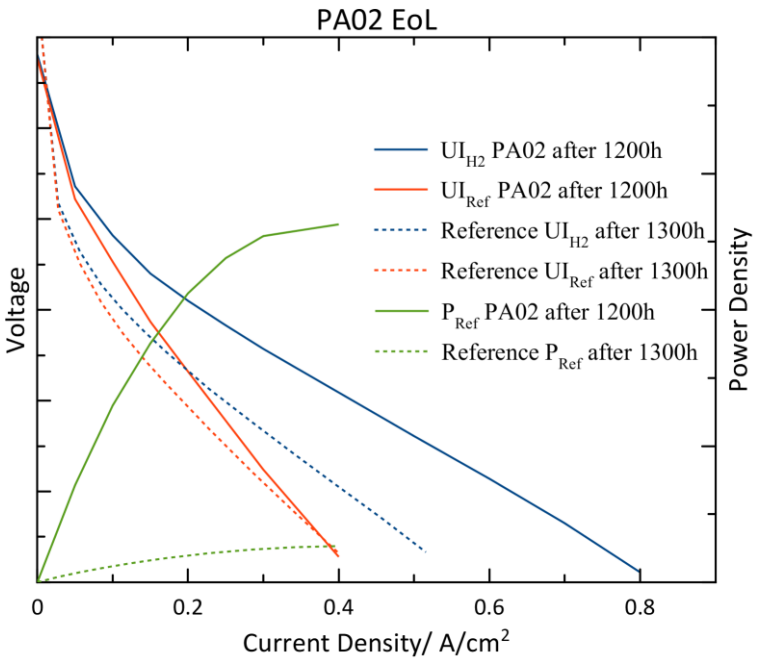

Figure 34: EoL UI characteristics of PA02 at 160 °C and 0.2 A.

It is apparent from both the long term test and the UI characteristics (Figure 32-33) that the functionalisation with PANI significantly improves the activity and the stability of the electrodes. While the non-functionalised reference electrode lost a significant amount of its original activity, the PANI layer on PA02 protects the electrode and upholds its activity even after 2000 h of operation.

4.5.3 PA03

Figure 35 illustrates the BoL CV of PA03. The ECSA of PA03 at BoL is 148 cm^2/mg which is 21% higher than the reference electrode without PANI.

The long term test of PA03 is shown in Figure 36. PA03 exhibits a potential of 6_{20} mV from the start of the test and 600 mV after 450 h of operation. Due to a malfunction of the H_2 MFC, there was a continuous shortage of H_2 in the cell which caused the drastic potential jumps illustrated in Figure 36 and a lower overall potential. Despite the shortage of H_2, the cell potential remained stable and dropped by only 20 mV after 450 h of operation.

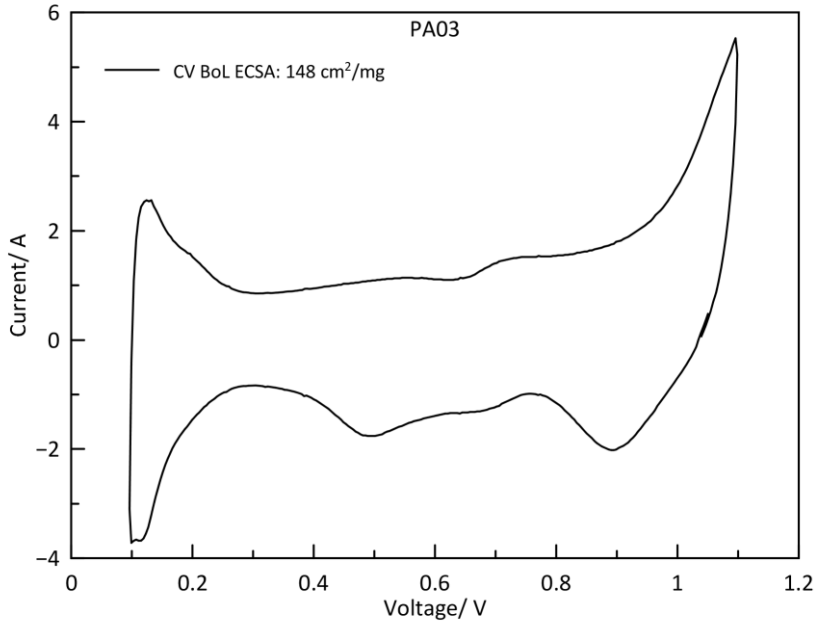

Figure 35: BoL CV of PA03.

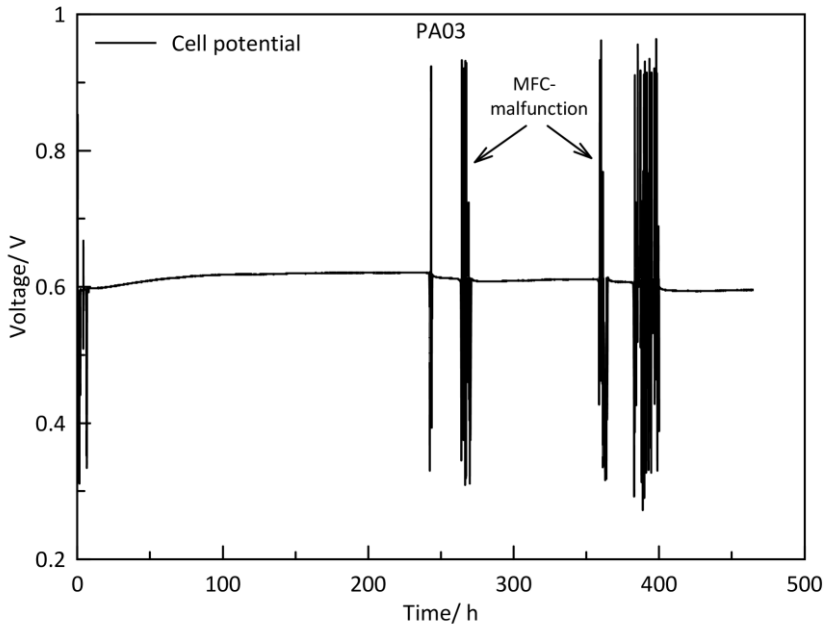

Figure 36: Long term test of PA03 at 160 °C and 0.2 A/cm².

Figure 37 illustrates the EoL CV of PA03. The ECSA of PA03 at EoL is 116 cm^2/mg which is 28% higher than the reference electrode without PANI.

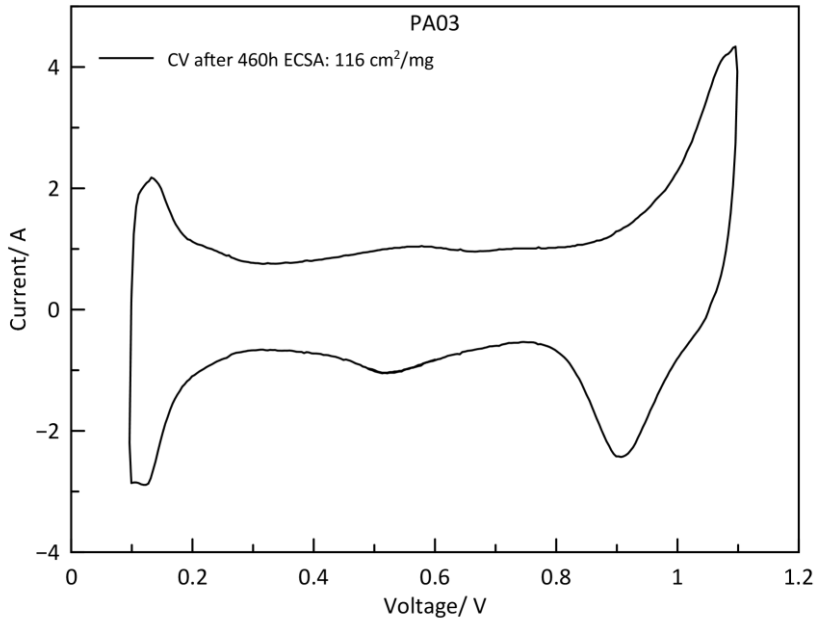

Figure 37: EoL CV of PA03.

Both the BoL and the EoL CV curves of PA03 show a higher ECSA than the reference electrode. The total losses of ECSA are similar for both PA03 and the reference electrode, 21% and 22%, respectively.

5 Summary and Outlook

The scope of this work was to increase the catalytic activity and stability of Pt based catalysts employed on the cathode side of HT-PEMFCs. PA, which originates from the polymer membrane, lowers the catalyst's activity towards the ORR by adsorbing on its surface and thus limits the performance of the FC. With the focus on improving the stability of the catalysts towards phosphate poisoning, commercial and in-house Pt based catalysts were functionalised with PANI using a straightforward synthesis method. PANI forms a thin film around the catalyst nanoparticles, mitigating phosphate adsorption. The prepared catalysts were electrochemically characterised using ex-situ methods. Additionally, pre-prepared GDEs were functionalised with PANI and tested in-situ in single cells.

For the preparation of the functionalised catalysts, aniline monomers were selectively adsorbed on the surface of the carbon support material. The PANI was deposited on commercial and in-house Pt/C and Pt-Co/C catalysts by an oxidative polymerisation of the aniline monomers. Additionally, using the same method, PANI was deposited on pure Vulcan XC72 in order to yield PANI functionalised support material (C@$PANI_{20}$) on which Pt NPs were then deposited, resulting in C@$PANI_{20}$+Pt_{20} and C@$PANI_{20}$+Pt_{50}. All commercial and in-house Pt/C, Pt-Co/C catalysts (Pt_{50}/C, Pt_{30}Co/C and $Pt_{22.5}$Co/C) as well as all PANI decorated catalysts (Pt_{30}Co/C@$PANI_{20}$, $Pt_{22.5}$Co/C@$PANI_{20}$, C@$PANI_{20}$+Pt_{20} and C@$PANI_{20}$+Pt_{50}) were characterised using a rotating disk electrode. CV and ORR measurements were performed in pure electrolyte as well as in 1 mM and 5 mM PA containing electrolyte.

Among all catalysts that were characterised via ex-situ methods, in-house C@$PANI_{20}$+Pt_{50} showed the most promising results regarding its ECSA in 1 mM and 5 mM PA containing electrolyte. In contrast to the other catalysts which forfeited their ECSA upon addition of PA in the electrolyte, the ECSA of C@$PANI_{20}$+Pt_{50} increased by 10% and 4% after addition of 1 mM and 5 mM PA, respectively. Additionally, C@$PANI_{20}$+Pt_{50} exhibited the highest MA in pure electrolyte as well as in 1 mM and 5 mM PA containing electrolyte (0.069 ± 0.015 A/mg, 0.043 ± 0.015 A/mg, 0.026 ± 0.015 A/mg, respectively).

No clear pattern could be observed in the case of the in-house and commercial Pt-Co/C catalysts. The in-house Pt_{30}Co/C@$PANI_{20}$ catalyst showed a much higher MA than Pt_{30}Co/C in pure electrolyte (0.052 ± 0.06 A/mg vs. 0.030 ± 0.01 A/mg, respectively). Commercial

$Pt_{22.5}Co/C$ on the other hand did not improve its activity towards the ORR after functionalisation with PANI, but shows a higher MA than $Pt_{22.5}Co/C@PANI_{20}$ (0.069 ± 0.02 A/mg vs. 0.058 ± 0.01 A/mg, respectively).

Very promising results were achieved with PANI decoration of the pre-prepared GDEs. The functionalised electrodes showed up to 28% higher ECSAs and significantly improved stability compared to the undecorated reference electrodes during the in-situ long term testing. The decorated electrodes upheld their catalytic activity for up to 2000 h of operation. EoL characterisation of PA01 and PA02 showed an increase in potential and power density of 3% and 20%, respectively, from their initial potential at 0.2 A/cm². The reference electrode showed potential losses of up to 12% and power density losses of up to 91% at 0.2 A/cm². The long term tests of PA01, PA02 and PA03 showed a much slower degradation rate compared to the undecorated reference electrode. For 900 h of operation, the potential of PA02 at 0.2 A/cm² had a significantly low degradation rate of 0.14% per 100 h. After 1300 h of operation, the undecorated reference electrode showed less catalytic activity, lower potentials and lower power densities than PA02 after 2000 h of operation.

In conclusion, a fast and simple method for the functionalisation of Pt based catalysts with PANI was proven to successfully mitigate problems associated with PA adsorption. In-house $C@PANI_{20}+Pt_{50}$, which was synthesised according to the second method, showed the highest MA in pure and in PA containing electrolyte of all ex-situ characterised catalysts. PANI was successfully deposited on GDEs which improved the electrode's long term stability and catalytic activity compared to non-functionalised equivalents. These results from both ex-situ and in-situ experiments show that PANI, through its electron interaction with Pt, can help to minimize the phosphate adsorption on Pt NPs and thus uphold the catalyst's activity in PA containing environments.

6 References

1. Nations, U. Conference of the Parties Report of the Conference of the Parties on its twenty-first session , held in Paris from 30 November to 13 December 2015 Addendum Part two : Action taken by the Conference of the Parties at its twenty-first session Contents Decisions adopted by the Conference of the Parties Decision Decision 1 / CP . 21 Adoption of the Paris Agreement. **1194,** 1–36 (2016).

2. U.S. Energy Information Administration. *International Energy Outlook 2016*. *International Energy Outlook 2016* **0484(2016),** (2016).

3. Stadler, I. Power grid balancing of energy systems with high renewable energy penetration by demand response. *Util. Policy* **16,** 90–98 (2008).

4. Kirubakaran, A., Jain, S. & Nema, R. K. A review on fuel cell technologies and power electronic interface. *Renew. Sustain. Energy Rev.* **13,** 2430–2440 (2009).

5. Chen, S. *et al.* Nanostructured Polyaniline-Decorated Pt/C@PANI20 Core − Shell Catalyst with Enhanced Durability and Activity. *J. Am. Chem. Soc.* 13252–13255 (2012).

6. Larminie, J. & Dicks, A. *Fuel cell systems explained*. *Fuel* (2003).

7. Kim, I. *et al.* Catalytic reactions in direct ethanol fuel cells. *Angew. Chemie - Int. Ed.* **50,** 2270–2274 (2011).

8. Barbir, F. PEM Fuel Cells. in *Fuel Cell Technology: Reaching Towards Commercialization* (ed. Sammes, N.) 27–51 (Springer London, 2006).

9. Winkler, W. & Nehter, P. Thermodynamics of Fuel Cells. 13–50 (2008).

10. Force, E. & Cell, F. *Cell Voltages , Polarisations and Performances*.

11. Chen, C. & Fuller, T. F. The effect of humidity on the degradation of Nafion® membrane. *Polym. Degrad. Stab.* **94,** 1436–1447 (2009).

12. Li, Y., Jiang, L., Wang, S. & Sun, G. Influence of phosphoric anions on oxygen reduction reaction activity of platinum, and strategies to inhibit phosphoric anion adsorption. *Cuihua Xuebao/Chinese J. Catal.* **37,** 1134–1141 (2016).

13. Barelli, L., Bidini, G., Gallorini, F. & Ottaviano, A. An energetic-exergetic analysis of a residential CHP system based on PEM fuel cell. *Appl. Energy* **88,** 4334–4342 (2011).

14. Colella, W. Design options for achieving a rapidly variable heat-to-power ratio in a combined heat and power (CHP) fuel cell system (FCS). *J. Power Sources* **106,** 388–396 (2002).

15. Zhang, J. *et al.* High temperature PEM fuel cells. *J. Power Sources* **160,** 872–891 (2006).

16. Li, Q. *et al.* Phosphate-Tolerant Oxygen Reduction Catalysts. *ACS Catal.* (2014).

17. Chandan, A. *et al.* High temperature (HT) polymer electrolyte membrane fuel cells (PEMFC) e A review. *J. Power Sources* **231,** 264–278 (2013).

18. Shao, Y., Yin, G., Wang, Z. & Gao, Y. Proton exchange membrane fuel cell from low temperature to high temperature: Material challenges. *J. Power Sources* **167,** 235–242 (2007).

19. Topalov, A. a. *et al.* Towards a comprehensive understanding of platinum dissolution in acidic media. *Chem. Sci.* **5,** 631 (2014).

20. Lim, J. *et al.* Applied Catalysis B : Environmental Oxygen reduction reaction on electrodeposited PtAu alloy catalysts in the presence of phosphoric acid. *"Applied Catal. B, Environ.* **165,** 495–502 (2015).

21. He, Q., Shyam, B., Nishijima, M., Ramaker, D. & Mukerjee, S. Mitigating phosphate anion poisoning of cathodic Pt/C catalysts in phosphoric acid fuel cells. *J. Phys. Chem. C* **117,** 4877–4887 (2013).

22. Gasteiger, H. A., Kocha, S. S., Sompalli, B. & Wagner, F. T. Activity benchmarks and requirements for Pt, Pt-alloy, and non-Pt oxygen reduction catalysts for PEMFCs. *Appl. Catal. B Environ.* **56,** 9–35 (2005).

23. Stephens, I. E. L., Bondarenko, A. S., Grønbjerg, U., Rossmeisl, J. & Chorkendorff, I. Understanding the electrocatalysis of oxygen reduction on platinum and its alloys. *Energy Environ. Sci.* **5,** 6744 (2012).

24. Schenk, A. *et al.* Platinum-cobalt catalysts for the oxygen reduction reaction in high temperature proton exchange membrane fuel cells e Long term behavior under ex-situ and in-situ conditions. *J. Power Sources* **266,** 313–322 (2014).

25. Stassi, A. *et al.* The effect of thermal treatment on structure and surface composition of Pt30Co electro-catalysts for application in PEMFCs operating under automotive conditions. *J. Power Sources* **208,** 35–45 (2012).

26. Loukrakpam, R. *et al.* Nanoengineered Pt30Co and PtNi catalysts for oxygen reduction reaction: An assessment of the structural and electrocatalytic properties. *J. Phys. Chem. C* **115,** 1682–1694 (2011).

27. Travitsky, N. *et al.* Pt-, PtNi- and Pt30Co-supported catalysts for oxygen reduction in PEM fuel cells. *J. Power Sources* **161,** 782–789 (2006).

28. Shao, Y., Sui, J., Yin, G. & Gao, Y. Nitrogen-doped carbon nanostructures and their composites as catalytic materials for proton exchange membrane fuel cell. *Appl. Catal. B Environ.* **79,** 89–99 (2008).

29. Antolini, E. Graphene as a new carbon support for low-temperature fuel cell catalysts. *Appl. Catal. B Environ.* **123–124,** 52–68 (2012).

30. Wang, X., Li, W., Chen, Z., Waje, M. & Yan, Y. Durability investigation of carbon nanotube as catalyst support for proton exchange membrane fuel cell. *J. Power Sources* **158,** 154–159 (2006).

31. Coutanceau, C., Croissant, M. J., Napporn, T. & Lamy, C. Electrocatalytic reduction of dioxygen at platinum particles dispersed in a polyaniline film. *Electrochim. Acta* **46,** 579–588 (2000).

32. Minoru Mizuhata, Masako Oga, S. D. Preparation of Pt/polypyrrole Loaded Carbon Composite in Order to Improve Electrode Durability for Fuel Cells. *ECS Trans* **2,** 63–72 (2007).

33. Baturina, O. A. & Swider-lyons, K. E. Experimental Methods for Quantifying the Activity of Platinum Electrocatalysts for the Oxygen. *Anal. Chem.* **82,** 6321–6328 (2010).

34. Zhou, R., Zheng, Y., Jaroniec, M. & Qiao, S.-Z. Determination of the Electron Transfer

Number for the Oxygen Reduction Reaction: From Theory to Experiment. *ACS Catal.* **6,** 4720–4728 (2016).

35. Chen, S. *et al.* Supporting Information Nanostructured Polyaniline-Decorated Pt / C @ PANI Core – Shell Catalyst with Enhanced Durability and Activity. 1–12 (2012).

36. Holade, Y. *et al.* Electrochemical and Physicochemical Characterizations of Gold-Based Nanomaterials: Correlation between Surface Composition and Electrocatalytic Activity. *J. Electrochem. Soc.* **162,** H929–H937 (2015).

37. Kim, J., Park, S. & Kim, S. Capacitance behaviors of Polyaniline / Graphene Nanosheet Composites Prepared by Aniline Chemical Polymerization. *Carbon Lett.* **14,** 51–54 (2013).

7 Appendix

7.1 List of Figures

7.2 List of Tables